



This discussion paper is/has been under review for the journal Geoscientific Model Development (GMD). Please refer to the corresponding final paper in GMD if available.

High resolution air quality simulation over Europe with the chemistry transport model CHIMERE

E. Terrenoire¹, B. Bessagnet¹, L. Rouïl¹, F. Tognet¹, G. Pirovano², L. Létinois¹, A. Colette¹, P. Thunis³, M. Amann⁴, and L. Menut⁵

¹INERIS, Parc Technologique Alata, BP 2, 60550 Verneuil-en-Halatte, France

²RSE, Via Rubattino 54, 20134 Milano, Italia

³JRC, Via Enrico Fermi 2749, 21027 Ispra, Italia

⁴IIASA, Schlossplatz 1, 2361 Laxenburg, Austria

⁵Institut P.-S. Laplace, Laboratoire de Météorologie Dynamique, CNRS, UMR8539, Ecole Polytechnique, Palaiseau, France

Received: 28 June 2013 – Accepted: 25 July 2013 – Published: 2 August 2013

Correspondence to: E. Terrenoire (etienne.terrenoire@ineris.fr)

Published by Copernicus Publications on behalf of the European Geosciences Union.

GMDD

6, 4137–4187, 2013

High resolution air
quality simulation
over Europe

E. Terrenoire et al.

Title Page

Abstract

Introduction

Conclusions

References

Tables

Figures

⏪

⏩

◀

▶

Back

Close

Full Screen / Esc

Printer-friendly Version

Interactive Discussion



Abstract

A high resolution air quality simulation ($0.125^\circ \times 0.0625^\circ$ horizontal resolution) performed over Europe for the year 2009 has been evaluated using both rural and urban background stations available over most of the domain. Using seasonal and yearly mean statistical indicators such as the correlation index, the fractional bias and the root mean squared error; we interpret objectively the performance of the simulation. Positive outcomes are: a very good reproduction of the daily variability at UB sites for O_3 ($R = 0.73$) as well as for NO_2 ($R = 0.61$); a very low bias calculated at UB stations for $PM_{2.5}$ (FB = -6.4 %) and PM_{10} concentrations (FB = -20.1 %). Conversely, main weaknesses in model performance include: the underestimation of the NO_2 daily maxima at UB site (FB = -53.6 %); an overall underestimation of PM_{10} and $PM_{2.5}$ concentrations observed over Eastern European countries (e.g. Poland); the overestimation of sulphates concentrations at spring time (FB = 53.7 %); finally, over the year, total nitrate and ammonia concentrations are better reproduced than nitrate and ammonium aerosol phase compounds. Obtained results suggest that, in order to improve the model performances, efforts should focus on the improvement of the emission inventory quality for Eastern Europeans countries and the improvement of a specific parameterisation in the model to better account for the urban effect on meteorology and air pollutants concentrations.

1 Introduction

Chemistry-Transport Models (CTMs) were initially designed to simulate ozone concentrations within the lower troposphere and a coarse horizontal resolution was sufficient to reach this objective. During the last decade, the air quality legislation has focussed more and more on particulate matter (PM) concentrations and CTMs have been equipped with aerosol modules. High PM concentrations are usually observed in urban areas (EEA, 2012) leading to an increase of CTMs applications at urban scale.

GMDD

6, 4137–4187, 2013

High resolution air quality simulation over Europe

E. Terrenoire et al.

Title Page

Abstract

Introduction

Conclusions

References

Tables

Figures



Back

Close

Full Screen / Esc

Printer-friendly Version

Interactive Discussion



High resolution air quality simulation over Europe

E. Terrenoire et al.

Title Page

Abstract

Introduction

Conclusions

References

Tables

Figures

⏪

⏩

◀

▶

Back

Close

Full Screen / Esc

Printer-friendly Version

Interactive Discussion



The application field of CTMs is broad and includes: understanding of physico-chemical processes (Bessagnet et al., 2010; Hodzic et al., 2010; Jiménez-Guerrero et al., 2011), assessment of emission control scenarios (Coll et al., 2010), past and future global air pollution trends (re)production (Colette et al., 2011), chemical weather forecast cooperation (Balk et al., 2011; Kukkonen et al., 2012), GEMS (<http://www.gmes.info>), GMES-MACC (<http://www.gmes-promote.org>) as well as natural hazard emergency response (Colette et al., 2011, Matthias et al., 2012). Both the constant evolution of model parameterisations and the increased quality of input data, including meteorology and emissions, should foster frequent CTMs assessments. The evaluation process should be performed over comprehensive spatial and temporal data set in order to effectively quantify the model accuracy. A list of European model evaluation studies that took place during the last decade can be found in Pay et al. (2012a). The CHIMERE model itself had undergone several extensive evaluations (Vautard et al., 2007a; Van Loon et al., 2007).

However, we note that CTMs are usually applied either to wide domains at coarse resolution or at high resolution but over small domains. The aim of the study is twofold: (i) get an accurate picture of air quality in Europe, and (ii) to comprehensively evaluate a fine resolution ($0.0625 \times 0.125^\circ$) CHIMERE simulation throughout Europe using the largest set of monitoring stations available in 2009. In this study, the CHIMERE model has been improved in order to simulate the air quality at the urban scale. The analysis is performed for ozone (O_3), nitrogen dioxide (NO_2), PM_{10} (Particles with an aerodynamic diameter $< 10 \mu m$), $PM_{2.5}$ (Particles with an aerodynamic diameter $< 2.5 \mu m$) and PM (Particulate Matter) compounds such as sulphate (SO_4^{2-}), nitrate (NO_3^-), total nitrate ($HNO_3 + NO_3^-$), ammonium (NH_4^+) and total ammonia ($NH_3 + NH_4^+$).

Hence, the paper is organized as follows: Sect. 2 is devoted to the description of CHIMERE, the methodology used to prepare the anthropogenic emissions and the set of observations used for the evaluation. Then, Sect. 3 describes and analyses comprehensively the ability of the model to reproduce the different selected pollutant

model (Guenther et al., 2006). We also account for wildfire emissions issued from the GFED3 (Kaiser et al., 2012).

2.2 Meteorology

Meteorological data needed by CHIMERE were derived from ECMWF-IFS fields. The choice of feeding CHIMERE directly with ECMWF-IFS stems from the results of a sensitivity analysis comparing the performance of WRF limited area model and the ECMWF-IFS (<http://www.ecmwf.int/research/ifsdocs>) against observed data. The analysis put in evidence a systematic overestimation of the wind speed by WRF, a feature confirmed also by other authors (Mass and Ovens, 2011; Jimenez and Dudhia, 2012). As an example, we draw the scatter plot of observed wind speeds (m s^{-1}) against IFS (red dots) and GFS/WRF (green dots) modelled values for European regional stations (Fig. 1) and it clearly shows that WRF enhances the wind speeds by 25 % on average over the selected period (January 2009). Furthermore, the direct use of ECMWF-IFS fields allows to avoid an ad-hoc meteorological numerical weather calculation. For more details the reader is referred to Miglietta et al. (2012).

The IFS model has a 0.25° horizontal grid spacing from surface to 0.1 hPa (91 levels in total). It delivers typical meteorological variables (temperature, wind components, specific humidity, pressure, sensible and latent heat fluxes) that need to be vertically and horizontally interpolated on the CHIMERE grid (8 levels). Some additional variables are also diagnosed from the available fields, such as friction velocity and vertical wind speed, used to complete the description of vertical transport and turbulent diffusion.

However, the main limitation of such data is that the IFS regional scale data cannot represent correctly the urban scale meteorology observed in the urban canopy layer and the urban sub-layer. This is crucial as the urban canopy is affecting the wind circulation and the urban energy balance (Sarrat et al., 2006) that will directly impact the transport and the vertical diffusion of primary pollutants over cities (e.g. O_3 , NO_2 and PM). In order to integrate the influence of the urban canopy on meteorology, the

High resolution air quality simulation over Europe

E. Terrenoire et al.

Title Page

Abstract

Introduction

Conclusions

References

Tables

Figures

◀

▶

◀

▶

Back

Close

Full Screen / Esc

Printer-friendly Version

Interactive Discussion



wind speed and the vertical diffusion (K_z coefficient) are modified within the CHIMERE version used for this study. Usually, operational meteorological observations are performed outside urban areas (e.g. airport) for representativeness reasons. Some study reveals large differences between urban and rural winds (Fisher et al., 2006) showing a wind speed ratio (rural/urban) up to a factor two. Another study shows that within the modeling case of Lisbon the ratio between wind speed inside the canopy and at the top of the urban sub-layer was within the range 0.1 to 0.6 (Solazzo et al., 2010).

In order to estimate the potential impact of the wind and dispersion coefficient (K_z) urban correction, we performed a sensitivity test over January 2009. Figure 2 shows the difference in concentration between the simulations with and without the urban correction for four main pollutants: NO_2 , O_3 , PM_{10} and $\text{PM}_{2.5}$. For all examined pollutants, we note a rather strong impact over all major European cities. For NO_2 , we observe an increase in concentration ranging from a few ppb (suburban areas) to 12–15 ppb (e.g. Paris, London, Madrid and Milan). Consecutively to the NO_2 concentrations increase over cities, we note a decrease of O_3 (NO_2 titration essentially), not only over the main cities (5 ppb on average up to 7 ppb in the city centre), but also over medium size cities (1 to 2 ppb). However the strongest impact is observed for the PM and especially for the PM_{10} where an increase from a few to $40 \mu\text{g m}^{-3}$ for cities such as Milan or Paris is seen but up to $70 \mu\text{g m}^{-3}$ for the region of Katowice in south Poland.

2.3 Anthropogenic emissions

The anthropogenic emission pre-processor transforms raw yearly anthropogenic emissions (ton/year/cells) into a CHIMERE compliant spatialised emission dataset. The raw emission data of the main air pollutants (Non Methanic Volatile Organic Compound (NMVOC), NO_x , CO, SO_2 , NH_3 , PPM) come from the annual inventory that is delivered by the European Monitoring and Evaluation Program (EMEP) (Vestreng, 2003). Emissions are provided per activity sector, according to the level 1 of the Selected Nomenclature for Air Pollution (SNAP) classification:

High resolution air quality simulation over Europe

E. Terrenoire et al.

Title Page

Abstract

Introduction

Conclusions

References

Tables

Figures



Back

Close

Full Screen / Esc

Printer-friendly Version

Interactive Discussion



High resolution air quality simulation over Europe

E. Terrenoire et al.

Title Page

Abstract

Introduction

Conclusions

References

Tables

Figures

◀

▶

◀

▶

Back

Close

Full Screen / Esc

Printer-friendly Version

Interactive Discussion

1. Combustion in energy and transformation industries
2. Non-industrial combustion plants
3. Combustion in manufacturing industry
4. Production processes
5. Extraction and distribution of fossil fuels and geothermal energy
6. Solvent and other product use
7. Road transport
8. Other mobile sources and machinery
9. Waste treatment and disposal
10. Agriculture
11. Other sources and sinks

Figure 3 displays the five main steps that can be identified in the anthropogenic emission pre-processing (1) the spatial regridding of the raw emission to comply with the CHIMERE grid, (2) the temporal disaggregation, (3) the chemical speciation, (4) the hourly disaggregation and (5) the surface flux calculation within CHIMERE.

2.3.1 Spatial re-gridding of anthropogenic emissions

The first step of emission processing consists in regridding the EMEP anthropogenic emission inventory available over a $0.5^\circ \times 0.5^\circ$ resolution grid onto the CHIMERE computational grid using a set of suitable proxy variables. We derived most of these variables from the US Geological Survey (USGS) Land Uses database, whose high resolution (1 km) preserves the accuracy in term of emission spatialisation. Twenty height

landuse categories exist in the USGS database but only “crops”, “grasslands”, “urbanized area” and “forest” are used to downscale the emissions.

For this study, the emission pre-processor has been modified to allow emissions from SNAP 2 to be disaggregated according to the population density. The goal of this approach is to better capture the spatial variability of the SNAP 2 emissions sector. The population data were provided by the Joint Research Centre (JRC) over a regular grid at $0.083 \times 0.083^\circ$ horizontal resolution. For the elaboration of the SNAP 2 emissions, we also made a distinction between gaseous and PPM species to better reallocate the anthropogenic biomass burning emissions (SNAP 2) over the rural areas. Indeed, according to the French national spatialised emission inventory, available at municipality level and derived using the bottom-up approach (MEDDTL, Ministère de l'Ecologie et du Développement Durable, 2004), there is clear evidence that $\text{PPM}_{2.5}$ emissions per inhabitant sharply decrease when the population density increases (Fig. 4). This is due to the increase of the relative contribution of wood burning in the fuel mixture moving from urban centres to rural areas (e.g. due to increase in domestic fireplaces). This effect is noticeable only for $\text{PPM}_{2.5}$, because biomass burning emissions are less influent on gas phase pollutant than particulate matter. Finally, total emissions used in CHIMERE are computed by simply averaging the emission fluxes from each landuse/population cell belonging to the same “mother” CHIMERE cell.

As an illustration, Fig. 5 shows the spatial distribution of the $\text{PPM}_{2.5}$ emissions from the SNAP 2 sector derived from the EMEP emission inventory. The picture shows the total annual primary particle emission $< 2.5 \mu\text{m}$ obtained from SNAP 2 using the pre-described modifications. Compared to the original method, we observe that around the medium and large size cities SNAP 2 emissions using the population proxy are increased. This is due to the fact that when using the landuse proxy, emissions from each type of Land Use (LU) cells have the same weight, thus giving rise to a flatter distribution than using population. Considering for example an EMEP cell including a big city as well as a small town, emissions are modulated in the same way over urban

High resolution air quality simulation over Europe

E. Terrenoire et al.

Title Page

Abstract

Introduction

Conclusions

References

Tables

Figures



Back

Close

Full Screen / Esc

Printer-friendly Version

Interactive Discussion



cells of both areas if we follow the LU approach, whereas, most of the emissions are allocated just in the big city if population is used.

The vertical repartition of the emission into the different levels of the CTM is known to be of great importance (Bieser et al., 2011). It is calculated according to the SNAP sector for each primary pollutant of the inventory following the calculation of Bieser et al. (2011) (Table 1). We also add a new layer (0–40 m) compared to the original EMEP setting. Note that for SNAP 2, 6, 7, 8 and 10 all the emissions are released into the first level of the model.

2.3.2 Chemical speciation

Annual NO_x emissions were speciated into NO , NO_2 and HNO_2 using the coefficients recommended by IASA (personal communication, Table 2). For NMVOC, a speciation was performed over 32 NMVOCs NAPAP (National Acid Precipitations Assessment Program) classes (Middleton et al., 1990). In a second time, an aggregation step is performed to lump NMVOCs into model species following Middleton et al. (1990). Time disaggregation was done on the basis of GENEMIS data using monthly, weekly and hourly coefficients depending on the activity sector (Society et al., 1994). Finally, hourly values of surface anthropogenic emissions are available for PPM and 15 primary gaseous pollutants: NO , NO_2 , CO , SO_2 , CH_4 , and the ten following NMVOC: Ethane, n-butane, ethene, propene, oxylene, formaldehyde, acetaldehyde, methyl, ethyl-ketone, ethanol and ethanol.

2.3.3 SNAP 2 emission temporal modulation

For SNAP 2, we also propose a new temporal profile derived according to the daily degree day concept. The degree day is an indicator used as a proxy variable to express the daily energy demand for heating. The degree day for a day “ j ” is defined as: $D_j = \max(0, 20 - T_D)$ where T_D is the daily mean 2 m temperature. Therefore, a first guess daily modulation factor could be defined as: $F_d = D_j / \overline{D}$ with \overline{D} the annual aver-

Title Page

Abstract

Introduction

Conclusions

References

Tables

Figures

◀

▶

◀

▶

Back

Close

Full Screen / Esc

Printer-friendly Version

Interactive Discussion



aged degree day. Considering that SNAP 2 emissions are not only related to the air temperature (e.g. emissions due to production of hot tap water), a second term is introduced in the formula by means of a constant offset C . To better assess the influence of this offset, C can be expressed as a fraction of \bar{D} (degree day annual average).

5 Considering:

$$C = A\bar{D} \text{ where } A = 0.1 \text{ (defined by user),}$$

the daily modulation factor (F_j) is therefore defined as:

$$F_j = D'_j / \bar{D}' \text{ where } D'_j = D_j + A\bar{D} \text{ and } \bar{D}' = (1 + A)\bar{D}$$

Note that F is mass conservative over the year and replaces the original monthly and daily modulation factors.

10 As an illustration, Fig. 6 shows the 2009 daily modulation factor applied to the SNAP 2 emissions at three locations both geographically and climatically different: Katowice (Poland), Paris (France) and Madrid (Spain). We observe that the highest factors for the three locations are logically seen during the winter period and the lowest ones during
15 the summer. This means, for example, that during the cold periods the emission from SNAP 2 can be up to three times more intense (e.g. beginning of January for Madrid or end of February for Paris) than during the spring or the autumn periods. Interestingly, we note that in Katowice during the beginning of the year the factors are relatively lower than at the two other locations meaning that over this period the difference between the
20 daily mean temperature and the annual mean is lower in Katowice than at the two other locations. In other words, Madrid and Paris experienced a cold period in January and at the end of February, respectively, whose intensity with respect to the climatology was higher than in Katowice. Inversely, at the end of the year, all locations experienced a cold outbreak of the same intensity relatively to their local annual mean temperature.

High resolution air quality simulation over Europe

E. Terrenoire et al.

Title Page

Abstract

Introduction

Conclusions

References

Tables

Figures



Back

Close

Full Screen / Esc

Printer-friendly Version

Interactive Discussion



2.4 Observation data

Observed data come from two different databases. The first one is Airbase (<http://acm.eionet.europa.eu/databases>) gathering regulatory data reported by Member States according to the air quality directive. The second one is related to the EMEP network (<http://www.emep.int/>). Only stations below 750 m in altitude with 75% data capture over the year are selected. Figure 7 displays the spatial distribution of the AIRBASE (green squares for Rural Background (RB) and blue dots for Urban Background (UB)), EMEP stations (red triangles) used for the evaluation. The stations spatial repartition is homogenous over the populated regions of western Europe, while several gaps are noted in Eastern European and in the Balkans countries. Table 3 shows that a high number of stations is available for most of the pollutants in which we are interested in (NO_2 , O_3 and PM_{10}). Differently, we note that fewer stations are available for $\text{PM}_{2.5}$ both at UB sites (267) and especially at RB sites (92). The EMEP database includes less sites than Airbase, but it is the only European network providing PM speciation data, that are crucial to investigate in deeper detail the model performance. Details about the station type classifications and the different measurements techniques are available through the previously quoted Airbase and EMEP websites.

2.5 Data analysis methodology

In this paper, we perform an “operational evaluation” (Dennis et al., 2010). The evaluation is based on the comparison of observation and modelled values using statistical indicators and graphic methods. We have selected different statistical indicators for their ability to diagnose the model performance from different perspectives including temporal correlation, bias, absolute error, agreement between observation and modelled values. Therefore, along with the observed (OM) and modelled (MM) mean concentration, we calculate: the observed (σ_{obs}) and modelled (σ_{mod}) standard deviation, the correlation index (R), the root mean square error (RMSE), the fractional bias (FB), the fractional error (FE) and the index of agreement (IA). Details about the calcula-

GMDD

6, 4137–4187, 2013

High resolution air quality simulation over Europe

E. Terrenoire et al.

Title Page

Abstract

Introduction

Conclusions

References

Tables

Figures

◀

▶

◀

▶

Back

Close

Full Screen / Esc

Printer-friendly Version

Interactive Discussion



tion of the statistics, performed using the Atmospheric Model Evaluation Tool software (AMET) can be found in Appel et al. (2011). The performance evaluation is based on yearly and seasonal statistics using the hourly (AIRBASE) and daily (EMEP) values of all stations available for the given typology (UB and RB).

3 Model results

Tables 4 and 5 display the different yearly and seasonal statistical scores for NO_2 , O_3 , PM_{10} , and $\text{PM}_{2.5}$ at RB and UB Airbase stations respectively. Table 6 displays the same metrics computed at EMEP sites, thus including also for sulphate (SO_4^{2-}), nitrate (NO_3^-), total nitrate ($\text{HNO}_3 + \text{NO}_3^-$), ammonium (NH_4^+) and total ammonia ($\text{NH}_3 + \text{NH}_4^+$). Figures 8 and 9 show the daily box-whisker plots time series of the NO_2 , O_3 , PM_{10} and $\text{PM}_{2.5}$ species computed at RB and UB stations, respectively. Figure 10 shows the box-whisker plots time series for sulphate (SO_4^{2-}), total nitrate ($\text{HNO}_3 + \text{NO}_3^-$), total ammonia ($\text{NH}_3 + \text{NH}_4^+$) calculated using the EMEP stations.

3.1 Nitrogen dioxide

Figures 8 and 9 show that along the year, CHIMERE catches nicely the temporal variability of NO_2 both at RB ($R = 0.68$) and UB ($R = 0.61$) sites. At UB stations, it underestimates significantly the concentrations over the year ($\text{FB} = -53.6\%$) and especially during the winter season ($\text{FB} = -63.9\%$). This behaviour is also observed at RB sites with however a lower bias ($\text{FB} = -46.5\%$ in the winter). The quantiles calculations allow to conclude that at RB sites, the lowest values are the best reproduced while at UB the model underestimates the observed percentile by 50%. For UB sites, the poor performance can be explained by the general tendency to underestimate NO_x urban emissions (e.g. Eastern European cities) whose impact is magnified by the winter stagnant conditions that increase the NO_2 observed concentrations at ground level (e.g. 5–20 January). Further investigation of the model behaviour over urban areas performed

Title Page

Abstract

Introduction

Conclusions

References

Tables

Figures

⏪

⏩

◀

▶

Back

Close

Full Screen / Esc

Printer-friendly Version

Interactive Discussion



using the DELTA tool (Thunis et al., 2012), pointed out that the performance was significantly higher over the main European cities (e.g. capitals) UB stations than over the UB stations of medium and small cities. Figure 11 shows the scatter plot of the modelled versus observed NO₂ concentrations ($\mu\text{g m}^{-3}$) at the UB stations ($N = 105$) of 30 major cities across Europe. The blue dot represents the mean of the 105 UB stations. We note that the use of those selected stations reduces significantly the bias between observed and modelled concentrations from 4.58 ppb when using all UB available stations to 1.31 ppb when using only major cities UB stations (factor 3.5). This indicates that the urban correction is not sufficient to correctly capture the NO₂ concentrations which remain underestimated over small cities. At this point of the study, the reasons for this underestimation remain unclear and could be due to the yet too coarse horizontal resolution to correctly simulate the urban meteorology over small cities as well as the spatial gradient of the emissions.

Nevertheless, at RB sites the interpretation of the negative bias is more difficult to explain. A possible explanation could be inferred noting that CHIMERE usually performs better in reproducing the temporal variability of the observed concentrations (e.g. standard deviation and correlation index) than the mean values. This result seems to indicate a lack in the oxidised nitrogen burden, due to an underestimation of the NO_x emissions.

3.2 Ozone

Overall, the daily temporal variability of O₃ concentrations is very well simulated both at rural ($R = 0.77$) and UB sites ($R = 0.73$) (Figs. 8 and 9, respectively). The comparison of the quantiles of the modelled and observed concentrations shows that the highest values are well reproduced while lower quantile are overestimated. Indeed, the modelled values show a systematic positive bias which is higher at UB (FB = 25.2 %) than at RB sites (20.1 %). At urban sites, this tendency can be related to the lack of O₃ titration by NO₂ due to the previously described underestimation of NO₂ especially during the winter. The bias has a seasonal variation with low positive FB that is observed at

Title Page

Abstract

Introduction

Conclusions

References

Tables

Figures



Back

Close

Full Screen / Esc

Printer-friendly Version

Interactive Discussion



UB sites in the summer (14.9%) and a high one during the winter (35.6%). A similar tendency is seen at RB sites but with a lower magnitude. The RMSE indicator also confirms the fact that at UB sites the model has a tendency to overshoot the maxima during the winter. However, at RB sites, the RMSE stays rather constant over the entire year (8.5 ppb in mean). The tendency is likely to be related to the overestimation of the background concentrations by CHIMERE as previously described in Chen et al. (2003) and Szopa et al. (2009).

3.3 PM₁₀ and PM_{2.5}

The model correctly reproduces the PM_{2.5} concentration at both RB and UB (FB = -6.4%) sites for all seasons. The only exception is during the winter where the FB gets higher (-24.6% at UB stations). At UB sites, the *R* index is better in autumn (0.69) than in summer (0.46). At RB sites the FB is always positive except during winter (-8.7%) and the maximum is observed during the autumn (14.2%) and the minimum during the summer (0.4%). The highest correlation index is observed at RB sites during the winter (0.74). Note that the overestimation of PM_{2.5} at RB sites is limited to the lowest values, as shown by the low quantile of the modelled concentrations.

The PM₁₀ performance for the model is good too (FB = -20.10% at UB station over the year) though slightly worse than for PM_{2.5}. At UB stations, we note that the FB is lower during the warm season (-12.2% at spring time) than in winter (-36.6%). *R* gets its highest values during the autumn (0.56) and its lowest value during summer and winter (0.47). At RB sites, over the year, the model agrees better in terms of correlation compared to the UB sites (0.62 against 0.52 at UB sites) and especially during winter (0.67 against 0.47 at UB stations) than during summer (0.50 against 0.47 at UB sites). It is worth noting that the RMSE is increasing by a factor two on average in the winter compared to the other seasons during which it stays rather constant (e.g. 34.8 μg m⁻³) during the winter and 17.33 μg m⁻³ at spring at UB sites). A strong inter-seasonal variability is observed with the lowest FB noted during the summer for PM₁₀ (-2.3%) and PM_{2.5} (5.8%) and the highest during winter for PM₁₀ (-14.4%) and

during autumn for PM_{2.5} (15.7%). As observed at the RB Airbase stations, the highest correlation coefficient is found during the winter for both PM₁₀ (0.68) and PM_{2.5} (0.77). Similarly, the highest RMSE error is found during the winter for PM₁₀ (12.3 ppb) and PM_{2.5} (10.7 ppb).

The comparison of PM₁₀ and PM_{2.5} model performance show that the highest yearly *R* index is calculated for PM_{2.5} at both UB (0.65) and RB sites (0.71). It indicates that on a yearly basis, CHIMERE reproduces better the temporal variability of PM_{2.5} across Europe than the PM₁₀ one. In both cases, we also observe that CHIMERE performed better in reproducing the low PM₁₀ and PM_{2.5} concentrations as shown by the quantiles. Overall, the better performance of the model for PM_{2.5} confirms that the underestimation mainly relies on the PM coarse modelling.

PM₁₀, PM_{2.5} and PM speciation data are available for several EMEP sites. As previously observed at the Airbase RB stations, CHIMERE overestimates the PM_{2.5} concentrations at the EMEP RB stations (Table 6). Interestingly, by opposition to the Airbase RB stations, the PM₁₀ are also overestimated at EMEP RB stations (FB = 2.9%). Such differences in model performance points out that RB of EMEP and Airbase networks are characterized by a different representativeness, being the latter more influenced by local scale emissions. This is confirmed also by comparing the main statistics of the observed PM₁₀ and PM_{2.5} data set whose the observed mean and σ are always lower at EMEP-RB sites than at Airbase-RB sites.

As the model performance for PM₁₀ is reflected by the quality of the reproduction of its different components, we also look at the capacity of the model to reproduce three main PM compounds: sulphate, nitrate and ammonium species.

3.4 Sulphate

Sulphuric acid is produced from the oxidation of sulphur oxides, which in turn form sulphate particle. Secondary sulphate aerosol occurs predominantly in the accumulation mode; diameter between 0.1 and 1.0 μm (Altshuller, 1982). Both oxidants and SO₂ availability are the limited factors for sulphate formation. In 2009, the 37 stations

GMDD

6, 4137–4187, 2013

High resolution air
quality simulation
over Europe

E. Terrenoire et al.

Title Page

Abstract

Introduction

Conclusions

References

Tables

Figures

⏪

⏩

◀

▶

Back

Close

Full Screen / Esc

Printer-friendly Version

Interactive Discussion



available over Europe indicate that the highest concentrations are measured during winter and spring (Fig. 10 and Table 6). This tendency is reproduced by the model ($R = 0.57$ during spring and 0.52 during the winter) but some maxima are overestimated especially during spring, autumn and winter. Consequently, the FB is rather low during the summer (FB = 20.1 %) but indicates a strong overestimation during spring time (FB = 53.7 %). This tendency is in opposition with the one calculated by CALIOPE (Pay et al., 2012a) and CMAQ (Matthias et al., 2008). Conversely to CHIMERE, CALIOPE and CMAQ tend to underestimate the sulphate surface concentrations over Europe along the year.

If we look at the seasonal trend, CHIMERE is in agreement with the study of Baker and Scheff, 2007 in North America with a minimum observed during the summer but it is in opposition with what is observed over Spain using the CMAQ model (Pay et al., 2012a). In this case, the highest sulphate concentrations occur in summer due to high oxidation of SO_2 during this period. In order to explain the overestimation of sulphate by CHIMERE, we looked at a remote RB station located in Ireland at the boundary of the domain and called Valencia observatory (51.94°N ; 10.24°W). The yearly time-series shows at this site an overestimation of $0.40 \mu\text{g m}^{-3}$ in mean over the year. This bias compares to the one between the modelled and measured values ($0.34 \mu\text{g m}^{-3}$) calculated over the whole domain (Table 6). As this station is away from any anthropogenic emission sources, the global overestimation of sulphate is very likely to be caused by an overestimation of the sulphate boundary conditions.

3.5 Particulate and total nitrate

Nitrogen dioxide (NO_2) and nitric acid (HNO_3) are the two main gas precursors that can react together to form ammonium nitrate (NH_4NO_3) depending on the temperature and the relative humidity (RH) (Ansari and Pandis, 1998). Nitric acid can be produced either through homogeneous reaction of NO_2 with OH radical (daytime), reaction of NO_3 with aldehydes or hydrocarbons (daytime) or hydrolysis of N_2O_5 in the troposphere (night time) (Richards, 1983; Russell et al., 1986). Note that at cold temperatures, the

Title Page

Abstract

Introduction

Conclusions

References

Tables

Figures

⏪

⏩

◀

▶

Back

Close

Full Screen / Esc

Printer-friendly Version

Interactive Discussion



equilibrium of the NH_4NO_3 system shifts towards aerosol phase. At low RH, ammonium nitrate is solid but if RH overcomes the deliquescence threshold it turns to aqueous phase ($\text{NH}_4^+ + \text{NO}_3^-$) (Bauer et al., 2011).

Sulphuric acid plays a crucial role in the formation of nitrate and ammonium. Sulphate tends to react preferentially with ammonia to form $(\text{NH}_4)_2\text{SO}_4$. Two regimes can be identified: the ammonia poor and the ammonia rich regime (Bauer et al., 2011). In the first case, there is not enough NH_3 to neutralize the available sulphate. In the second case, sufficient ammonia is present to neutralize the sulphate and the remaining ammonia is available to react with nitrate to produce NH_4NO_3 .

Using the 17 EMEP stations, we show that the nitrates are strongly underestimated along the year (FB = -103.5%) but a rather high R value is noted during the winter (0.67) indicating the good reproduction of the temporal variability of nitrate concentrations by CHIMERE during this period (Table 6). The lowest FB is observed during the winter (-68.4%). Winter is also linked to the highest measured and modelled nitrate concentrations. During cold periods, the formation of NH_4NO_3 is favoured and the associated low dispersive conditions enhance the increase of nitrate during these periods. Different explanations concerning the general underestimation of nitrate can be considered. First, the underestimation could be explained by the previously described overestimation of sulphate in poor ammonia regimes. Secondly, the coarse nitrate chemistry is not represented in the CHIMERE version used leading to an underestimation of the coarse mode nitrate aerosol. This process was however implemented during a research project in CHIMERE (Hodzic et al., 2006). Typical reactions involved in the coarse nitrate chemistry include the neutralisation of acidic aerosol particle (NO_3^-) by different basic positive ions such as Ca^{2+} and Mg^{2+} . Na^+ and Cl^- are also involved along coastal areas where high sea salt (NaCl) concentrations are observed. Differently, the total nitrate concentrations (Fig. 10) are much better reproduced than the nitrate alone ($R = 0.66$ during the winter) except during the summer ($R = 0.16$). The order of magnitude of the FB indicates an underestimation of 80% in mean over the year. Thus, TNO_3 is better reproduced by the model than NO_3^- but it is still underestimated.

High resolution air quality simulation over Europe

E. Terrenoire et al.

Title Page

Abstract

Introduction

Conclusions

References

Tables

Figures

⏪

⏩

◀

▶

Back

Close

Full Screen / Esc

Printer-friendly Version

Interactive Discussion



This result is coherent with the NO₂ underestimation previously discussed, thus confirming a possible lack in NO_x emissions.

3.6 Particulate and total ammonia

Along with sulphate, ammonium appears to be the best SIA compound reproduced by CHIMERE (Table 6). The FB is rather low (27.1 % over the year) and shows the lowest overestimation during the summer (7.5%). This overestimation could also be driven by the corresponding overestimation of the sulphate. Note that associated to a good correlation index (0.77), winter is the season during which CHIMERE best reproduces the observations. A similar tendency is also noted when using the CMAQ model over Spain and the UK (Pay et al., 2012b; Chemel et al., 2010).

Similarly, the total ammonia (Fig. 10) is nicely reproduced by CHIMERE with a very low bias observed during winter (FB = -1.8%). The performance is decreasing during summer during which the model is underestimating observations (FB = -10.7%). Differently from TNO₃, the total NH₃ is rather well reproduced, suggesting that the yearly NH₃ emissions are well estimated. However, the temporal profile of NH₃ still needs to be improved. In that sense, recent work concerning the improvement the temporal variability as well as the magnitude and the spatial distribution of NH₃ emissions from the agricultural sector had been done for France (Hamaoui-Laguel et al., 2012). Unfortunately, a robust monthly time-profile for the NH₃ emission from fertilizer is yet to be finalized for Europe (Menut and Bessagnet, 2010) before its implementation in the model.

3.7 Spatio-temporal variability of the modelled concentration fields

In this section, we analyse the 2-D annual mean concentrations maps of NO₂, O₃, PM₁₀ and PM_{2.5} (Fig. 12). On each map, the observed values for each station are represented by a coloured dot. We also draw the winter (December-January-February) and the summer (June-July-August) seasonal means to analyse the inter-seasonal

GMDD

6, 4137–4187, 2013

High resolution air
quality simulation
over Europe

E. Terrenoire et al.

Title Page

Abstract

Introduction

Conclusions

References

Tables

Figures

⏪

⏩

◀

▶

Back

Close

Full Screen / Esc

Printer-friendly Version

Interactive Discussion



variability of the modelled concentrations for NO₂ and O₃ (Fig. 13), PM₁₀ and PM_{2.5} (Fig. 14) and SIA species (Figs. 15 and 16).

NO₂ concentrations are directly linked to emissions mainly from SNAP 2 (non-industrial combustion plants), 7 (road traffic) and 8 (other mobile source). Figure 12 therefore shows that the highest annual mean concentrations are located over urban area and along ship tracks (Atlantic, Channel, and Mediterranean Sea). We identify specific areas with high concentrations: the Pô-Valley, Paris, Benelux, London, southern Poland (e.g. Katowice), Athens, Madrid and Barcelona. For those specific areas and generally over Europe the concentrations are much higher during winter than during summer due to higher emissions and low vertical dispersion (e.g. shallow boundary layer, low dispersion conditions, thermal inversion) (Fig. 13). Ship tracks in the Mediterranean Sea, the coast of Portugal and especially the Channel are characterised by rather high NO₂ annual modelled concentrations between 2 and 12 ppb. The observation values represented by the dots show a slight overall underestimation of the NO₂ concentrations. However two main areas located over the south of Poland (Katowice) and some parts of Romania (industrial hot spots) show a stronger underestimation (10–20 ppb). We also note some areas where the observations are overestimated: Paris, London, Madrid, Barcelona and Athens. For those areas, the methodology used to downscale the national annual emission could be the reasons of such a feature.

Generally we note that CHIMERE slightly overestimates the O₃ concentrations over Europe. Figure 12 shows that the highest annual mean concentrations are located below the 45° latitude where the strongest photolysis over Europe occurs (from 30 ppb over the coasts to 48 ppb over the sea). The O₃ maximum is modelled during summer while the winter seasonal mean is below 30 ppb over most of Europe reaching near zero values in the Benelux, the Pô Valley, Germany and Poland. The highest summer concentrations are calculated over and around the Mediterranean Sea where low boundary layer heights (as compared to continental PBL heights) and strong photolysis are favourable conditions to high ozone concentrations (up to 56 ppb). Note that

GMDD

6, 4137–4187, 2013

High resolution air quality simulation over Europe

E. Terrenoire et al.

Title Page

Abstract

Introduction

Conclusions

References

Tables

Figures

⏪

⏩

◀

▶

Back

Close

Full Screen / Esc

Printer-friendly Version

Interactive Discussion



during the warm period most of the capitals across Europe are characterised by ozone decrements due to the ozone titration by NO_x in those urbanised areas (Fig. 13).

For PM_{10} , the overall picture shows that the highest concentrations (from 20 to $30 \mu\text{g m}^{-3}$) are located at the south of a line which goes from the south of Portugal to the north of Poland (Fig. 12). The annual mean concentrations are nicely modelled (slight underestimation) over the continent except over cities such as Milan, Paris and Krakow where CHIMERE overestimates the observations. In winter, the calculated concentrations are maximal over the continent (between 10 and $30 \mu\text{g m}^{-3}$) with lower concentrations over central Spain ($10 \mu\text{g m}^{-3}$). Hot spots are located over the main European cities and over industrial primary emissions areas (e.g. Romania and Bulgaria). In summer, the concentrations are strongly influenced by the boundary condition dust level in the south part of the domain (up to $40 \mu\text{g m}^{-3}$) and the city signal is really low except for Katowice, Milan and Paris (up to $40 \mu\text{g m}^{-3}$) (Fig. 14). Over the continent the concentrations are lower by a factor of two. In winter, much lower concentrations are modelled over the Mediterranean Sea ($16\text{--}18 \mu\text{g m}^{-3}$) where the influence of dust at the boundary condition is the lowest while primary emissions from the main cities and industrial areas have their strongest intensity. Three hot spots can be identified: the Po valley, the south of Poland (Katowice region) and the south of Romania (area of Bucharest). Indeed, very high PM_{10} concentrations are modelled all over the year over those areas. The strong primary emissions (both SNAP 2 and 7) are the main reasons for this critical situation as well as favourable meteorological conditions for SIA formation (low vertical and horizontal dispersion and high level of humidity during the cold seasons) that play also a major role in the build up of high PM_{10} concentrations especially in the Pô valley.

For $\text{PM}_{2.5}$ (Figs. 12 and 14), the pattern is similar to the one described for PM_{10} . The highest concentrations are calculated all along the year over the Pô valley (30 to $60 \mu\text{g m}^{-3}$) except in summer (16 to $20 \mu\text{g m}^{-3}$). Note that, in spring, high concentrations are calculated over the east of the Mediterranean Sea and are partially linked to the production of sulphate in the fine aerosol mode. The observations show a good

GMDD

6, 4137–4187, 2013

High resolution air quality simulation over Europe

E. Terrenoire et al.

Title Page

Abstract

Introduction

Conclusions

References

Tables

Figures

◀

▶

◀

▶

Back

Close

Full Screen / Esc

Printer-friendly Version

Interactive Discussion



agreement with the modelled concentrations fields but a general underestimation is clearly identified over some Eastern Europe countries such as Poland and Bulgaria.

For sulphate (Fig. 15), during the winter, a sharp zonal gradient is observed with minima observed in Western Europe ($2 \mu\text{g m}^{-3}$ on average) and maxima in Eastern Europe (up to $8 \mu\text{g m}^{-3}$). The highest concentrations are located near the main SO_2 emission areas which correspond to the industrial areas in Romania, Bulgaria, Bosnia, Serbia, Hungary and south Poland that used sulphur-rich coal (e.g. in the Katowice region). In summer, the gradient is meridional with a maximum along the coast of northern Africa. In summer, sulphate resulting from the gas oxidation of SO_2 occurs in the Mediterranean Sea, where emissions from ships are high and intense photolysis allows production of oxidant radicals (e.g. OH radical).

For ammonium and nitrate (Fig. 16) a strong seasonal variability is modelled with lower concentrations in the summer and higher ones in winter. Nitrate is less influenced by its precursors emissions than sulphate. However, we note that larger modelled concentrations are seen during the winter over the Pô valley (up to $15 \mu\text{g m}^{-3}$), over the Benelux ($6 \mu\text{g m}^{-3}$) and the south of Germany ($8 \mu\text{g m}^{-3}$). High ammonium concentrations are also modelled over the Pô valley (up to $5.2 \mu\text{g m}^{-3}$) and other countries such as the Benelux, south of Germany, Poland, Hungary and the south of Romania where concentrations can reach $3.0 \mu\text{g m}^{-3}$.

4 Conclusions

A high resolution air quality CHIMERE simulation ($7 \times 7 \text{ km}$) over most of Europe has been evaluated using both rural and urban background stations for the year 2009. In this CHIMERE version, the main updates and model developments include:

- the use of the population density proxy to downscale the SNAP 2 emissions,
- the update of the emission layer depths and vertical emission injection heights,
- a new NO_x speciation,

GMDD

6, 4137–4187, 2013

High resolution air quality simulation over Europe

E. Terrenoire et al.

Title Page

Abstract

Introduction

Conclusions

References

Tables

Figures

◀

▶

◀

▶

Back

Close

Full Screen / Esc

Printer-friendly Version

Interactive Discussion



- the modulation of the SNAP2 emission according to the 2 m air temperature,
- the urban correction of Kz and wind speed variables.

Different seasonal and yearly mean statistical indicators have been calculated to objectively interpret the CHIMERE performances. We find out that increasing the resolution down to 7×7 km enable us to catch nicely the temporal variability ($R > 0.60$) for the main pollutants (NO_2 , O_3 , PM_{10} and $\text{PM}_{2.5}$) at urban sites. Additionally, we wish to underline that although the model performs slightly better at reproducing the concentrations at RB sites (except for $\text{PM}_{2.5}$), the performance is still very good at UB sites for O_3 (FB = 25.2 %) and PM_{10} (FB = -20.1 %). Conversely, for $\text{PM}_{2.5}$ the FB is lower and negative at UB sites (-6.4 %) compared to the RB sites (7.5 %). The modelled PM component concentration shows an overestimation of the sulphate that very likely limit the formation of the nitrate and the ammonium that are underestimated by the model. Moreover, we note that the total nitrate is also underestimated confirming the likely NO_x emissions underestimation. Finally, differently from the TNO_3 , the total burden of reduced nitrogen is rather well reproduced by the model indicating that the yearly NH_3 emissions are well estimated even if the temporal profile of NH_3 still needs to be improved

Therefore, three main areas of work have been identified in order to improve the CHIMERE performance:

- the development of CHIMERE urban parameterisations to account for the urban effect on meteorology and therefore on both the primary and secondary air pollutant concentrations,
- the introduction of the coarse nitrate chemistry and an advanced parameterisation accounting for wind-blow dust emissions,
- the introduction of existing national bottom-up approach emission databases (e.g. France, Spain) into the existing European emission inventory (e.g. MACC) for major cities and eastern European countries.

High resolution air quality simulation over Europe

E. Terrenoire et al.

Title Page

Abstract

Introduction

Conclusions

References

Tables

Figures

◀

▶

◀

▶

Back

Close

Full Screen / Esc

Printer-friendly Version

Interactive Discussion



Appendix A

Definition of the statistical indicators used for the evaluation

$$OM = \frac{1}{N} \sum_{t=1}^N \text{obs} \quad (\text{A1})$$

$$MM = \frac{1}{N} \sum_{t=1}^N \text{mod} \quad (\text{A2})$$

$$\sigma_{\text{obs}} = \frac{1}{N} \sum_{t=1}^N \sqrt{(\text{obs}(x, t) - \overline{\text{obs}(x)})^2} \quad (\text{A3})$$

$$\sigma_{\text{mod}} = \frac{1}{N} \sum_{t=1}^N \sqrt{(\text{mod}(x, t) - \overline{\text{mod}(x)})^2} \quad (\text{A4})$$

$$FB = \frac{1}{N} \sum_{t=1}^N \frac{\text{mod}(x, t) - \text{obs}(x, t)}{(\text{obs}(x, t) + \text{mod}(x, t))/2} \quad (\text{A5})$$

$$FE = \frac{1}{N} \sum_{t=1}^N \frac{|\text{mod}(x, t) - \text{obs}(x, t)|}{(\text{obs}(x, t) + \text{mod}(x, t))/2} \quad (\text{A6})$$

High resolution air quality simulation over Europe

E. Terrenoire et al.

$$R = \frac{\sum_{t=1}^N (\text{mod}(x, t) - \overline{\text{mod}(x)}) \cdot (\text{obs}(x, t) - \overline{\text{obs}(x)})}{\sqrt{\sum_{t=1}^N (\text{mod}(x, t) - \overline{\text{mod}(x)})^2} \sqrt{\sum_{t=1}^N (\text{obs}(x, t) - \overline{\text{obs}(x)})^2}} \quad (\text{A7})$$

$$\text{IA} = 1 - \frac{\sum_{t=1}^N (\text{mod}(x, t) - \text{obs}(x, t))^2}{\sum_{t=1}^N (|\text{mod}(x, t) - \overline{\text{obs}(x)}| - |\text{obs}(x, t) - \overline{\text{obs}(x)}|)^2} \quad (\text{A8})$$

$$\text{RMSE} = \sqrt{\frac{1}{N} \sum_{t=1}^N (\text{mod}(x, t) - \text{obs}(x, t))^2} \quad (\text{A9})$$

5 $\text{mod}(x, t)$ – computed concentration; $\text{obs}(x, t)$ – observed concentration; N – number of pairs.

A cut-off threshold has been applied to the observed concentrations to avoid numerical problems due to unrealistic observations. Thresholds have been defined as follows:

$$10 \text{ NO}_2 = 0.5 \text{ ppb}; \text{O}_3 = 5 \text{ ppb}; \text{PM}_{10} = 1 \mu\text{g m}^{-3}; \text{PM}_{2.5} = 1 \mu\text{g m}^{-3}.$$

$$\text{SO}_4^{2-} = 0.01 \mu\text{g m}^{-3}; \text{NO}_3^- = 0.01 \mu\text{g m}^{-3}; \text{NH}_4^+ = 0.01 \mu\text{g m}^{-3}.$$

$$\text{TNO}_3^- = 0.01 \mu\text{g m}^{-3}; \text{TNH}_4^+ = 0.01 \mu\text{g m}^{-3}.$$

15 *Acknowledgements.* This study was partly funded by the French Ministry in charge of Environment. This work was done under the auspices of the European project EC4MACS (EU LIFE, www.ec4macs.eu).

Title Page

Abstract

Introduction

Conclusions

References

Tables

Figures

◀

▶

◀

▶

Back

Close

Full Screen / Esc

Printer-friendly Version

Interactive Discussion



References

- Altshuller, A. P.: Atmospheric concentrations and distributions of chemical substances, in: the Acidic Deposition Phenomenon and its Effects, US Environmental Protection Agency, Washington, DC, 1982.
- 5 Ansari, A. S. and Pandis, S. N.: Response of Inorganic PM to Precursor Concentrations, *Environ. Sci. Technol.*, 32, 2706–2714, 1998.
- Appel, K. W., Gilliam, R. C., Davis, N., and Zubrow, A.: Overview of the Atmospheric Model Evaluation Tool (AMET) v1.1 for evaluating meteorological and air quality models, *Environ. Modell. Softw.*, 26, 434–443, 2011.
- 10 Baker, K. and Scheff, P.: Photochemical model performance for PM_{2.5} sulphate, nitrate, ammonium, and precursor species SO₂, HNO₃, and NH₃ at background monitor locations in the Central and Eastern United States, *Atmos. Environ.*, 41, 6185–6195, 2007.
- Balk, K., Kukkonen, J., Karatzas, K., Bassoukos, T., and Epitropou, V.: A European open access chemical weather forecasting portal, *Atmos. Environ.*, 45, 6917–6922, 2011.
- 15 Bauer, S. E., Koch, D., Unger, N., Metzger, S. M., Shindell, D. T., and Streets, D. G.: Nitrate aerosols today and in 2030: a global simulation including aerosols and tropospheric ozone, *Atmos. Chem. Phys.*, 7, 5043–5059, doi:10.5194/acp-7-5043-2007, 2007.
- Bessagnet, B., Menut, L., Curci, G., Hodzic, A., Guillaume, B., Liousse, C., Moukhtar, S., Pun, B., Seigneur, C., and Schulz, M.: Regional modeling of carbonaceous aerosols over Europe – Focus on Secondary Organic Aerosols, *J. Atmos. Chem.*, 61, 175–202, 2009.
- 20 Bessagnet B., Seigneur, C., and Menut, L.: Impact of dry deposition of semi-volatile organic compounds on secondary organic aerosols, *Atmos. Environ.*, 44, 1781–1787, doi:10.1016/j.atmosenv.2010.01.027, 2010.
- Bieser, J., Aulinger, A., Matthias, V., Quante, M., and Denier van der Gon, H. A. C.: Vertical emission profiles for Europe based on plume rise calculations, *Environ. Pollut.*, 159, 2935–2946, doi:10.1016/j.envpol.2011.04.030, 2011.
- 25 Chen, K. S., Ho, Y. T., Lai, C. H., and Chou, Y.-M.: Photochemical modeling and analysis of meteorological parameters during ozone episodes in Kaohsiung, Taiwan, *Atmos. Environ.*, 37, 1811–1823, 2003.
- 30 Colette, A., Favez, O., Meleux, F., Chiappini, L., Haeffelin, M., Morille, Y., Malherbe, L., Papin, A., Bessagnet, B., Menut, L., Leoz, E., and Rouil, L.: Assessing in near real time the impact

High resolution air quality simulation over Europe

E. Terrenoire et al.

Title Page

Abstract

Introduction

Conclusions

References

Tables

Figures

◀

▶

◀

▶

Back

Close

Full Screen / Esc

Printer-friendly Version

Interactive Discussion



High resolution air quality simulation over Europe

E. Terrenoire et al.

Title Page

Abstract

Introduction

Conclusions

References

Tables

Figures

◀

▶

◀

▶

Back

Close

Full Screen / Esc

Printer-friendly Version

Interactive Discussion



of the April 2010 Eyjafjallajökull ash plume on air quality, *Atmos. Environ.*, 45, 1217–1221, 2011.

Coll, I., Lasry, F., Fayet, S., Armengaud, A., and Vautard, R.: Simulation and evaluation of 2010 emission control scenarios in a Mediterranean area, *Atmos. Environ.*, 43, 4194–4204, 2009.

5 EEA: Air quality in Europe – 2012 report, EEA Report No 4/2012, Office for Official Publications of the European Union, ISBN 978-92-9213-328-3, 2012.

Fisher, B., Kukkonen, J., Piringer, M., Rotach, M. W., and Schatzmann, M.: Meteorology applied to urban air pollution problems: concepts from COST 715, *Atmos. Chem. Phys.*, 6, 555–564, doi:10.5194/acp-6-555-2006, 2006.

10 Ginoux, P., Chin, M., Tegen, I., Prospero, J. M., Holben, B., Dubovik, O., and Lin, S.-J.: Sources and distributions of dust aerosols simulated with the GOCART model, *J. Geophys. Res.*, 106, 20255–20273, 2001.

Guenther, A., Karl, T., Harley, P., Wiedinmyer, C., Palmer, P. I., and Geron, C.: Estimates of global terrestrial isoprene emissions using MEGAN (Model of Emissions of Gases and Aerosols from Nature), *Atmos. Chem. Phys.*, 6, 3181–3210, doi:10.5194/acp-6-3181-2006, 2006.

Hamaoui-Laguel, L., Meleux, F., Beekmann, M., Bessagnet, B., Générumont, S., Cellier, P., and Létinois, L.: Improving ammonia emissions in air quality modelling for France, *Atmos. Environ.*, doi:10.1016/j.atmosenv.2012.08.002, 2012.

20 Hauglustaine, D. A., Hourdin, F., Jourdain, L., Filiberti, M.-A., Walters, S., Lamarque, J.-F., and Holland, E. A.: Interactive chemistry in the Laboratoire de Meteorologie Dynamique general circulation model: Description and background tropospheric chemistry evaluation, *J. Geophys. Res.*, 109, D04314, doi:10.1029/2003JD003,957, 2004.

Hodzic, A., Bessagnet, B., and Vautard, R.: A model evaluation of coarse-mode nitrate heterogeneous formation on dust particle, *Atmos. Environ.*, 40, 4158–4171, 2006.

25 Hodzic, A., Jimenez, J. L., Madronich, S., Canagaratna, M. R., DeCarlo, P. F., Kleinman, L., and Fast, J.: Modeling organic aerosols in a megacity: potential contribution of semi-volatile and intermediate volatility primary organic compounds to secondary organic aerosol formation, *Atmos. Chem. Phys.*, 10, 5491–5514, doi:10.5194/acp-10-5491-2010, 2010.

30 Jimenez, P. A. and Dudhia, J.: Improving the representation of resolved and unresolved topographic effects on surface wind in the WRF model, *J. Appl. Meteor. Climatol.*, 51, 300–316, 2012.

High resolution air quality simulation over Europe

E. Terrenoire et al.

Title Page

Abstract

Introduction

Conclusions

References

Tables

Figures

◀

▶

◀

▶

Back

Close

Full Screen / Esc

Printer-friendly Version

Interactive Discussion



Jiménez-Guerrero, P., Jorba, O., Pay, M. T., Montávez, J. P., Jerez, S., Gómez-Navarro, J. J., and Baldasano, J. M.: Comparison of two different sea-salt aerosol schemes as implemented in air quality models applied to the Mediterranean Basin, *Atmos. Chem. Phys.*, 11, 4833–4850, doi:10.5194/acp-11-4833-2011, 2011.

5 Kaiser, J. W., Heil, A., Andreae, M. O., Benedetti, A., Chubarova, N., Jones, L., Morcrette, J.-J., Razinger, M., Schultz, M. G., Suttie, M., and van der Werf, G. R.: Biomass burning emissions estimated with a global fire assimilation system based on observed fire radiative power, *Biogeosciences*, 9, 527–554, doi:10.5194/bg-9-527-2012, 2012.

10 Kukkonen, J., Olsson, T., Schultz, D. M., Baklanov, A., Klein, T., Miranda, A. I., Monteiro, A., Hirtl, M., Tarvainen, V., Boy, M., Peuch, V.-H., Poupkou, A., Kioutsioukis, I., Finardi, S., Sofiev, M., Sokhi, R., Lehtinen, K. E. J., Karatzas, K., San José, R., Astitha, M., Kallos, G., Schaap, M., Reimer, E., Jakobs, H., and Eben, K.: A review of operational, regional-scale, chemical weather forecasting models in Europe, *Atmos. Chem. Phys.*, 12, 1–87, doi:10.5194/acp-12-1-2012, 2012.

15 Mass, C. F. and Ovens, D.: Fixing WRF's high speed wind bias: a new subgrid scale drag parameterization and the role of detailed verification, 91st AMS Annual Meeting, Seattle, WA, available at: <http://ams.confex.com/ams/91Annual/webprogram/Paper180011.html> (last access: 3 November 2011), 2011.

20 Matthias, V.: The aerosol distribution in Europe derived with the Community Multiscale Air Quality (CMAQ) model: comparison to near surface in situ and sunphotometer measurements, *Atmos. Chem. Phys.*, 8, 5077–5097, doi:10.5194/acp-8-5077-2008, 2008.

25 Matthias, V., Aulinger, A., Bieser, J., Cuesta, J., Geyer, B., Langmann, B., Serikov, I., Mattis, I., Minikin, A., Mona, L., Quante, M., Schumann, U., and Weinzierl, B.: The ash dispersion over Europe during the Eyjafjallajökull eruption – Comparison of MAQ simulations to remote sensing and air-borne in-situ observations, *Atmos. Environ.*, 48, 184–194, doi:10.16/j.atmosenv.2011.06.077, 2012.

Menut, L. and Bessagnet, B.: Atmospheric composition forecasting in Europe, *Ann. Geophys.*, 28, 61–74, doi:10.5194/angeo-28-61-2010, 2010.

30 Menut, L., Goussebaile, A., Bessagnet, B., Khvorostiyannov, D., and Ung, A.: Impact of realistic hourly emissions profiles on modelled air pollutants concentrations, *Atmos. Environ.*, 49, 233–244, doi:10.1016/j.atmosenv.2011.11.05, 2012.

Menut, L., Bessagnet, B., Khvorostyanov, D., Beekmann, M., Blond, N., Colette, A., Coll, I., Curci, G., Foret, G., Hodzic, A., Mailler, S., Meleux, F., Monge, J.-L., Pison, I., Siour, G., Tur-

High resolution air quality simulation over Europe

E. Terrenoire et al.

Title Page

Abstract

Introduction

Conclusions

References

Tables

Figures

◀

▶

◀

▶

Back

Close

Full Screen / Esc

Printer-friendly Version

Interactive Discussion



quety, S., Valari, M., Vautard, R., and Vivanco, M. G.: CHIMERE 2013: a model for regional atmospheric composition modelling, *Geosci. Model Dev.*, 6, 981–1028, doi:10.5194/gmd-6-981-2013, 2013.

Middleton, P., Stockwell, W. R., and Carter, W. P.: Agregation and analysis of volatile organic compound emissions for regional modeling, *Atmos. Environ.*, 24, 1107–1133, 1990.

Miglietta, M., Thunis, P., Georgieva, E., Pederzoli, A., Bessagnet, B., Terrenoire, E., and Collette, A.: Evaluation of WRF model performance in different European regions with the delta-Fairmode evaluation tool, *Int. J. Environ. Pollut.*, 50, 83–97, 2012.

Pay, M. T., Jiménez-Guerrero, P., and Baldasano, J. M.: Assessing sensitivity regimes of secondary inorganic aerosol formation in Europe with the CALIOPE-EU modeling system, *Atmos. Environ.*, 51, 146–164, 2012a.

Pay, M. T., Jiménez-Guerrero, P., Jorba, O., Basart, S., Querol, X., Pandolfi, M., and Baldasano, J. M.: Spatio-temporal variability of concentrations and speciation of particulate matter across Spain in the caliope modeling system, *Atmos. Environ.*, 46, 376–396, 2012b.

Richards, L. W.: Comments on the oxidation of NO₂ to nitrate: day and night, *Atmos. Environ.*, 17, 397–402, 1983.

Russell, A. G., Cass, G. R., and Seinfeld, J. H.: On some aspects of night-time atmospheric chemistry, *Environ. Sci. Technol.*, 20, 1167–1172, 1986.

Sarrat, C., Lemonsu, A., Masson, V., and Guedalia, D.: Impact of urban heat island on regional atmospheric pollution, *Atmos. Environ.*, 40, 1743–1758, 2006.

Solazzo, E., Di Sabatino, S., Aquilina, N., Dudek, A., and Britter, R.: Coupling Mesoscale Modelling with a Simple Urban Model: The Lisbon Case Study, *Bound.-Lay. Meteorol.*, 137, 441–457, doi:10.1007/s10546-010-9536-6, 2010.

Szopa, S., Foret, G., Menut, L., and Cozic, A.: Impact of large scale circulation on European summer surface ozone and consequences for modelling forecast, *Atmos. Environ.*, 43, 1189–1195, 2009.

Thunis, P., Georgieva, E., and Pederzoli, A.: A tool to evaluate air quality model performances in regulatory applications, *Environ. Model. Softw.*, 38, 220–230, doi:10.1016/j.envsoft.2012.06.005, 2012.

Van Loon, M., Vautard, R., Schaap, M., Bergström, R., Bessagnet, B., Brandt, J., Builtjes, P. J. H., Christensen, J. H., Cuvelier, C., Graff, A., Jonson, J. E., Krol, M., Langner, J., Roberts, P., Rouil, L., Stern, R., Tarrasón, L., Thunis, P., Vignati, E., White, L., and Wind, P.: Evaluation

GMDD

6, 4137–4187, 2013

High resolution air quality simulation over Europe

E. Terrenoire et al.

Title Page

Abstract

Introduction

Conclusions

References

Tables

Figures

◀

▶

◀

▶

Back

Close

Full Screen / Esc

Printer-friendly Version

Interactive Discussion



of long-term ozone simulations from seven regional air quality models and their ensemble, Atmos. Environ., 41, 2083–2097, 2007.

5 Vautard, R., Bessagnet, B., Chin, M., and Menut, L.: On the contribution of natural Aeolian sources to particulate matter concentrations in Europe: testing hypotheses with a modelling approach, Atmos. Environ., 39, 3291–3303, 2005.

10 Vautard, R., Builtjes, P. H. J., Thunis, P., Cuvelier, K., Bedogni, M., Bessagnet, B., Honore C., Moussiopoulos, N., Pirovano, G., Schaap, M., Stern, R., Tarrason, L., and Van Loon, M.: Evaluation and intercomparison of Ozone and PM₁₀ simulations by several chemistry-transport models over 4 European cities within the CityDelta project, Atmos. Environ., 41, 173–188, 2007a.

15 Vautard, R., Maldi, M., Menut, L., Beekmann, M., and Colette, A.: Boundary layer photochemistry simulated with a two-stream convection scheme, Atmos. Environ., 41, 8275–8287, 2007b.

Vestreng, V.: Review and revision of emission data reported to CLRTAP, EMEP Status report, 2003.

High resolution air quality simulation over Europe

E. Terrenoire et al.

Table 1. Vertical emissions profiles (%) for each SNAP (S) sector.

Injection height (m)	20	92	184	324	522	781	1106
S1	0	0	0.25	51	45.3	3.25	0.2
S2	100	0	0	0	0	0	0
S3	6	16	75	3	0	0	0
S4	5	15	70	10	0	0	0
S5	2	8	60	30	0	0	0
S6	100	0	0	0	0	0	0
S7	100	0	0	0	0	0	0
S8	100	0	0	0	0	0	0
S9	0	0	41	57	2	0	0
S10	100	0	0	0	0	0	0
S11	100	0	0	0	0	0	0

Title Page

Abstract

Introduction

Conclusions

References

Tables

Figures

◀

▶

◀

▶

Back

Close

Full Screen / Esc

Printer-friendly Version

Interactive Discussion



High resolution air quality simulation over Europe

E. Terrenoire et al.

Title Page

Abstract

Introduction

Conclusions

References

Tables

Figures

⏪

⏩

◀

▶

Back

Close

Full Screen / Esc

Printer-friendly Version

Interactive Discussion



Table 2. NO_x speciation used in CHIMERE for the simulation.

	S1	S2	S3	S4	S5	S6	S7	S8	S9	S11
NO	95.0	95.0	95.0	95.0	95.0	95.0	83.5	90.0	95.0	95.0
NO ₂	4.5	4.5	4.5	4.5	4.5	4.5	15.0	9.2	4.5	4.5
HNO ₂	0.5	0.5	0.5	0.5	0.5	0.5	1.5	0.8	0.5	0.5

High resolution air quality simulation over Europe

E. Terrenoire et al.

Title Page

Abstract

Introduction

Conclusions

References

Tables

Figures

◀

▶

◀

▶

Back

Close

Full Screen / Esc

Printer-friendly Version

Interactive Discussion



Table 3. Number of stations available per species and network over the domain of simulation.

	NUMBER OF STATIONS		UNIT
	UB	RB	
AIRBASE			
NO ₂	770	300	ppb
O ₃	586	361	ppb
PM ₁₀	677	238	µg m ⁻³
PM _{2.5}	267	92	µg m ⁻³
EMEP			
NO ₂	X	24	ppb
PM ₁₀	X	21	µg m ⁻³
PM _{2.5}	X	17	µg m ⁻³
SO ₄ ²⁻	X	37	µgS m ⁻³
NO ₃ ⁻	X	17	µgN m ⁻³
TNO ₃	X	26	µgN m ⁻³
NH ₄ ⁺	X	17	µgN m ⁻³
TNH ₃	X	14	µgN m ⁻³

High resolution air quality simulation over Europe

E. Terrenoire et al.

Table 4. Annual and seasonal scores calculated using the whole RB Airbase set of stations. The statistics are: the Observed Mean (OM), the Modelled Mean (MM), the standard deviation of the observations (σ_{obs}) and modelled values (σ_{mod}), the correlation index (R), the Root Mean Squared Error (RMSE), the Fractional Bias (FB in %) and the Fractional Error (FE in %) and the Index of Agreement (IA). N_{OBS} is the number of observations. Units for each pollutant are reported in Table 3, R and IA are unit less. The statistical indicators selected for the operational evaluation are defined in Appendix A.

	N_{OBS}	OM	MM	σ_{obs}	σ_{mod}	R	RMSE	FB	FE	IA
NO₂										
Annual	98 833	6.55	4.63	5.75	4.37	0.68	4.67	-33.90	53.40	0.77
Spring	25 173	5.66	3.94	4.41	3.50	0.63	3.90	-37.90	56.10	0.74
Summer	24 168	4.22	3.27	3.15	2.60	0.53	2.97	-26.00	50.40	0.70
Autumn	24 929	6.58	5.04	4.97	4.56	0.67	4.20	-29.50	50.40	0.79
Winter	16 105	10.23	6.22	8.36	5.59	0.69	7.26	-46.50	59.30	0.74
O₃										
Annual	122 518	28.60	33.45	11.13	8.65	0.77	8.59	20.10	26.30	0.81
Spring	31 787	35.12	38.71	9.19	6.35	0.59	8.29	11.90	19.40	0.71
Summer	31 865	33.91	37.77	9.30	6.28	0.65	8.05	13.10	19.50	0.73
Autumn	30 074	23.50	30.26	9.74	7.12	0.71	9.64	30.60	34.90	0.72
Winter	18 941	21.65	27.56	8.68	8.08	0.70	8.82	27.40	33.10	0.75
PM₁₀										
Annual	77 828	20.67	17.90	14.93	9.65	0.62	12.02	-5.50	37.70	0.73
Spring	19 656	21.41	20.01	14.25	9.54	0.60	11.49	2.10	36.00	0.73
Summer	19 639	17.17	14.41	8.63	6.54	0.50	8.26	-13.30	35.70	0.68
Autumn	19 459	19.28	18.19	12.36	10.16	0.64	9.77	0.30	37.30	0.79
Winter	12 374	27.20	18.94	22.45	11.11	0.67	18.95	-20.30	43.60	0.68
PM_{2.5}										
Annual	27574	13.69	12.78	12.59	7.96	0.71	8.99	7.50	40.40	0.79
Spring	6737	14.80	14.71	12.05	7.44	0.67	8.95	13.20	39.10	0.76
Summer	7043	9.87	9.11	5.50	3.74	0.53	4.80	0.40	36.90	0.69
Autumn	7151	12.29	12.44	10.29	7.68	0.71	7.31	14.20	42.10	0.81
Winter	4186	20.05	15.16	19.78	10.70	0.74	14.73	-8.70	43.50	0.75

High resolution air quality simulation over Europe

E. Terrenoire et al.

Table 5. Annual and seasonal scores calculated using the whole UB Airbase set of stations. The indicators and the associated units are identical to the ones define in the Table 4.

	N_{OBS}	OM	MM	σ_{obs}	σ_{mod}	R	RMSE	FB	FE	IA
NO₂										
Annual	264 005	13.15	8.57	8.14	8.09	0.61	8.48	-53.60	66.60	0.73
Spring	67 205	12.34	7.91	6.93	7.71	0.59	8.02	-57.80	70.40	0.71
Summer	65 960	8.97	6.64	5.14	6.53	0.51	6.34	-44.00	63.70	0.68
Autumn	65 665	13.39	9.13	7.52	8.40	0.64	8.05	-51.70	64.00	0.74
Winter	42 984	18.65	10.77	9.98	9.15	0.64	11.37	-63.90	70.50	0.70
O₃										
Annual	190 716	24.90	30.71	10.95	9.43	0.73	9.62	25.20	33.40	0.79
Spring	51 219	30.31	35.30	9.21	7.91	0.56	9.54	16.90	25.90	0.69
Summer	51 195	31.08	35.29	9.36	7.28	0.62	8.60	14.90	22.70	0.73
Autumn	46 215	19.80	27.46	9.07	7.90	0.64	10.60	36.90	43.00	0.68
Winter	28 040	17.02	24.18	7.91	8.83	0.62	10.28	35.60	45.50	0.68
PM₁₀										
Annual	226 954	29.27	22.56	22.98	16.61	0.52	21.29	-20.10	40.80	0.66
Spring	57 618	28.65	24.03	18.59	13.89	0.50	17.33	-12.20	37.50	0.67
Summer	56 778	21.50	16.62	11.05	7.81	0.47	11.18	-22.40	38.60	0.63
Autumn	57 100	28.47	23.09	21.05	16.34	0.56	18.78	-16.80	39.80	0.71
Winter	36 494	41.45	26.59	34.55	23.83	0.47	34.88	-36.60	50.80	0.62
PM_{2.5}										
Annual	79 664	17.52	15.07	14.65	10.29	0.65	11.39	-6.40	37.80	0.76
Spring	20 200	17.28	16.59	12.53	8.36	0.59	10.16	5.20	36.10	0.72
Summer	20 093	11.91	10.05	6.13	4.28	0.46	5.94	-11.50	36.80	0.64
Autumn	20 932	16.46	14.65	12.43	9.74	0.69	9.26	-4.00	37.50	0.81
Winter	11 344	27.53	19.67	23.01	14.97	0.61	19.87	-24.60	43.30	0.70

Title Page

Abstract

Introduction

Conclusions

References

Tables

Figures

◀

▶

◀

▶

Back

Close

Full Screen / Esc

Printer-friendly Version

Interactive Discussion



Table 6. Annual and seasonal scores calculated using the RB EMEP stations. The indicators and the associated units are identical to the ones define in the Table 4. TNO₃ is the total nitrate (HNO₃+ NO₃⁻) and TNH₄ is the total ammonia (NH₃+NH₄⁺).

	N _{OBS}	OM	MM	σ_{obs}	σ_{mod}	R	RMSE	FB	FE	IA
PM₁₀										
Annual	6579	16.72	15.91	11.03	7.56	0.56	9.29	2.90	35.40	0.70
Spring	1697	18.26	18.11	12.08	8.47	0.49	10.83	7.20	35.20	0.66
Summer	1648	14.66	13.86	7.46	6.42	0.46	7.31	-2.30	32.10	0.67
Autumn	1620	15.25	15.93	8.80	7.75	0.65	6.98	9.80	35.30	0.80
Winter	1056	20.48	15.47	14.88	7.12	0.68	12.33	-14.40	39.40	0.68
PM_{2.5}										
Annual	4858	11.69	10.90	9.62	5.35	0.68	7.22	8.60	42.00	0.74
Spring	1242	13.27	12.71	10.48	5.74	0.62	8.28	12.30	41.60	0.70
Summer	1202	8.69	8.60	4.55	3.39	0.36	4.58	5.80	39.10	0.59
Autumn	1217	10.00	10.32	7.12	4.78	0.67	5.30	15.70	42.70	0.78
Winter	767	16.32	11.78	13.76	6.43	0.77	10.72	-11.60	45.70	0.72
SO₄²⁻										
Annual	10596	0.73	1.07	0.62	0.67	0.50	0.72	42.40	55.30	0.65
Spring	2830	0.75	1.19	0.54	0.56	0.57	0.67	53.70	60.80	0.66
Summer	2576	0.69	0.79	0.42	0.39	0.46	0.44	20.10	42.50	0.66
Autumn	2461	0.67	1.02	0.50	0.69	0.51	0.71	45.20	56.60	0.62
Winter	1872	0.88	1.22	0.96	0.84	0.52	0.95	43.40	57.60	0.68
NO₃⁻										
Annual	4647	0.64	0.32	1.49	0.53	0.28	1.47	-103.50	116.20	0.34
Spring	1201	0.88	0.38	2.38	0.62	0.24	2.36	-95.00	107.80	0.26
Summer	1148	0.46	0.08	1.47	0.19	0.13	1.50	-156.10	157.10	0.12
Autumn	1141	0.49	0.28	0.59	0.44	0.48	0.58	-99.40	113.30	0.63
Winter	763	0.76	0.54	0.72	0.68	0.67	0.61	-68.40	90.20	0.79
TNO₃										
Annual	7327	0.60	0.37	0.62	0.40	0.56	0.56	-55.10	71.60	0.67
Spring	1907	0.68	0.43	0.65	0.42	0.67	0.54	-50.70	66.80	0.74
Summer	1844	0.46	0.23	0.62	0.21	0.16	0.66	-66.50	75.10	0.30
Autumn	1742	0.55	0.35	0.42	0.35	0.62	0.39	-56.80	72.30	0.73
Winter	1209	0.77	0.51	0.73	0.55	0.66	0.62	-49.50	73.50	0.76
NH₄⁺										
Annual	5427	1.01	1.14	1.63	0.81	0.43	1.47	27.10	50.60	0.53
Spring	1409	1.25	1.31	2.45	0.81	0.35	2.30	31.90	51.60	0.37
Summer	1373	0.71	0.67	1.37	0.40	0.24	1.33	7.50	42.50	0.25
Autumn	1287	0.80	1.11	0.81	0.75	0.59	0.77	39.70	56.00	0.73
Winter	902	1.37	1.47	1.29	0.97	0.77	0.83	21.10	49.30	0.85
TNH₄										
Annual	4036	1.49	1.55	1.29	1.06	0.60	1.07	6.00	43.70	0.76
Spring	1036	1.66	1.91	1.30	1.26	0.58	1.20	14.30	43.20	0.74
Summer	1027	1.50	1.30	1.30	0.84	0.58	1.08	-10.70	35.90	0.70
Autumn	1005	1.43	1.54	1.34	1.02	0.61	1.08	10.80	44.90	0.76
Winter	629	1.47	1.41	1.28	0.96	0.69	0.93	-1.80	48.20	0.81

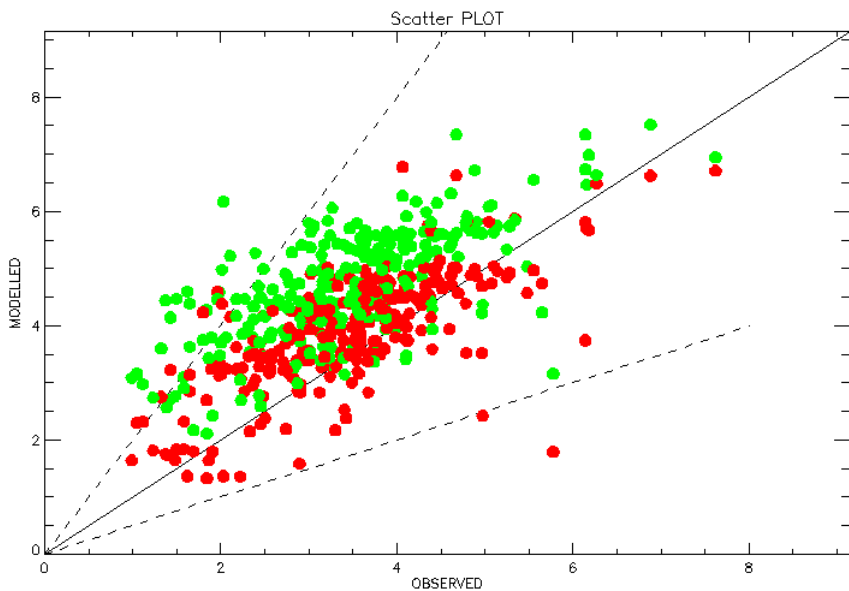


Fig. 1. Observed wind speeds (m s^{-1}) against IFS (red dots) and GFS/WRF (green dots) modelled values for rural background stations in January 2009.

High resolution air quality simulation over Europe

E. Terrenoire et al.

Title Page

Abstract

Introduction

Conclusions

References

Tables

Figures

◀

▶

◀

▶

Back

Close

Full Screen / Esc

Printer-friendly Version

Interactive Discussion

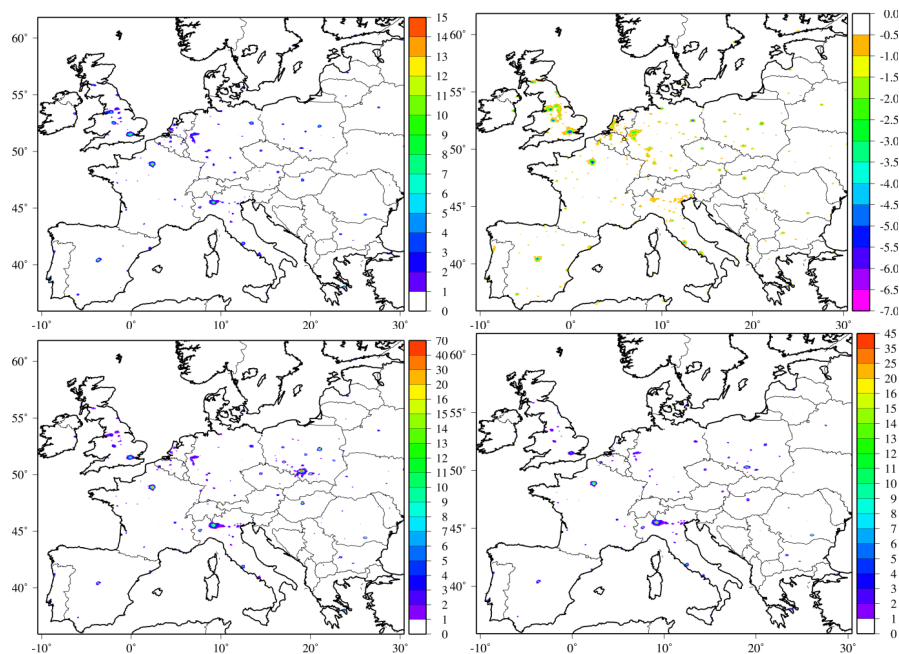


Fig. 2. Difference in concentrations for four main pollutants between the simulation using the urban correction and the simulation not using the urban correction for NO_2 in ppb (top left), O_3 in ppb (top right), PM_{10} in $\mu\text{g m}^{-3}$ (bottom left) and $\text{PM}_{2.5}$ $\mu\text{g m}^{-3}$ (bottom right).

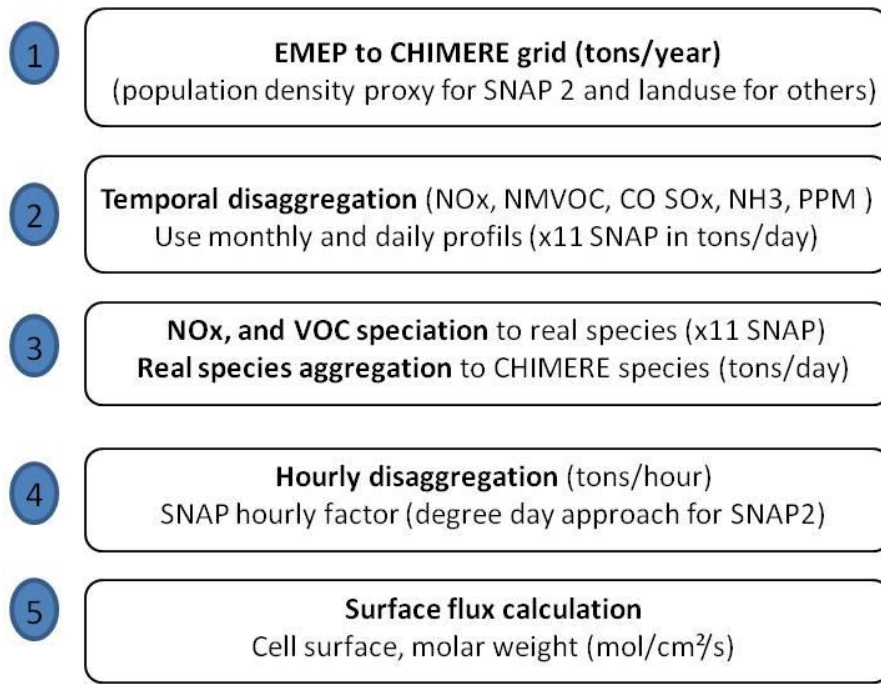


Fig. 3. The EMEP to CHIMERE emission converter (adapted from Menut et al., 2012).

High resolution air quality simulation over Europe

E. Terrenoire et al.

Title Page

Abstract Introduction

Conclusions References

Tables Figures

◀ ▶

◀ ▶

Back Close

Full Screen / Esc

Printer-friendly Version

Interactive Discussion



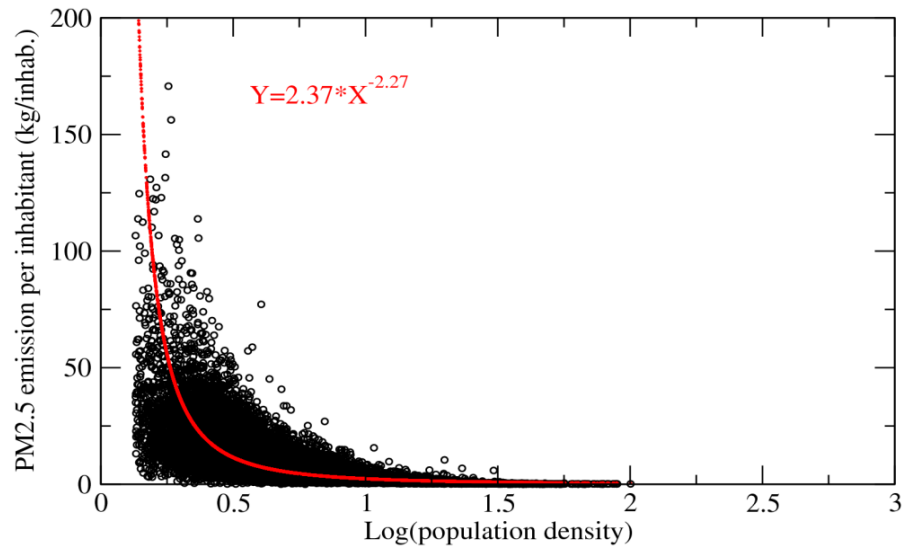


Fig. 4. Evolution of PM_{2.5} residential emissions per inhabitant (kg inh⁻¹ yr⁻¹) as a function of population density (source: French National Emission Inventory). The red curve is the corresponding logarithmic regression used in the CHIMERE emission pre-processor.

High resolution air quality simulation over Europe

E. Terrenoire et al.

[Title Page](#)

[Abstract](#) [Introduction](#)

[Conclusions](#) [References](#)

[Tables](#) [Figures](#)

[◀](#) [▶](#)

[◀](#) [▶](#)

[Back](#) [Close](#)

[Full Screen / Esc](#)

[Printer-friendly Version](#)

[Interactive Discussion](#)



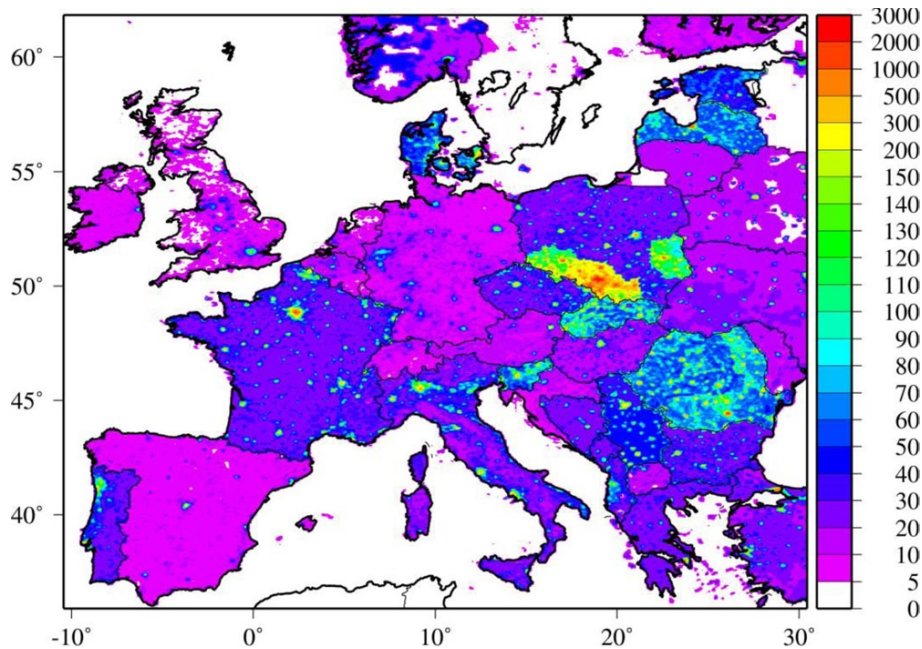


Fig. 5. Total annual primary particle emission with diameter below $2.5\ \mu\text{m}$ from SNAP 2 (g km^{-2}).

High resolution air quality simulation over Europe

E. Terrenoire et al.

Title Page

Abstract

Introduction

Conclusions

References

Tables

Figures

⏪

⏩

◀

▶

Back

Close

Full Screen / Esc

Printer-friendly Version

Interactive Discussion



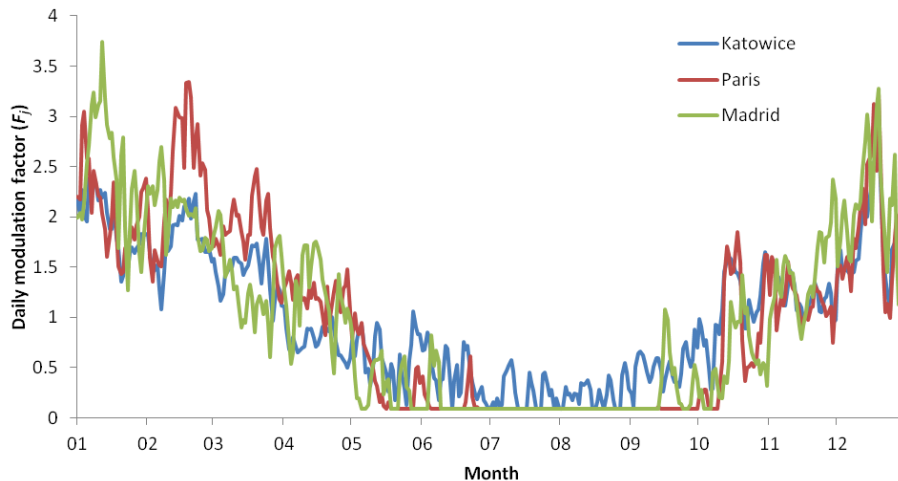


Fig. 6. Daily modulation factor (F_j) apply for the SNAP 2 emission over the city of Katowice, Paris and Madrid for the year 2009.

GMDD

6, 4137–4187, 2013

High resolution air quality simulation over Europe

E. Terrenoire et al.

[Title Page](#)

[Abstract](#) [Introduction](#)

[Conclusions](#) [References](#)

[Tables](#) [Figures](#)

[⏪](#) [⏩](#)

[◀](#) [▶](#)

[Back](#) [Close](#)

[Full Screen / Esc](#)

[Printer-friendly Version](#)

[Interactive Discussion](#)



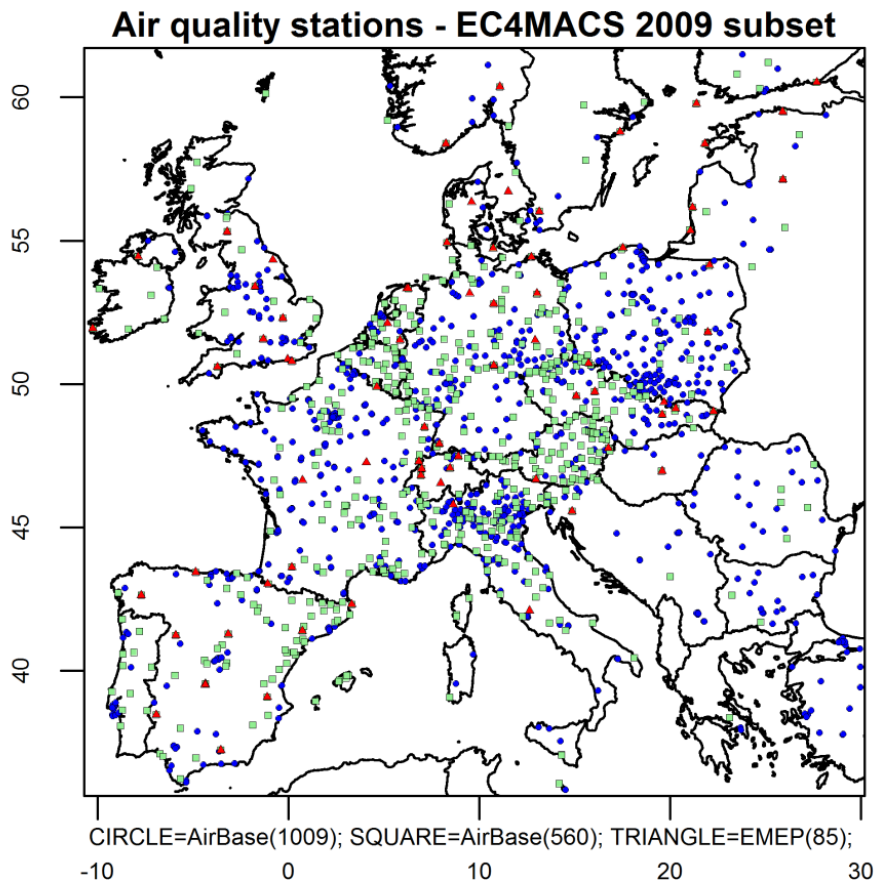


Fig. 7. Airbase RB (green squared), Airbase UB (blue dots) and EMEP stations (red triangles) projected on the simulation domain, used for the evaluation.

GMDD

6, 4137–4187, 2013

High resolution air quality simulation over Europe

E. Terrenoire et al.

Title Page

Abstract

Introduction

Conclusions

References

Tables

Figures



Back

Close

Full Screen / Esc

Printer-friendly Version

Interactive Discussion



High resolution air quality simulation over Europe

E. Terrenoire et al.

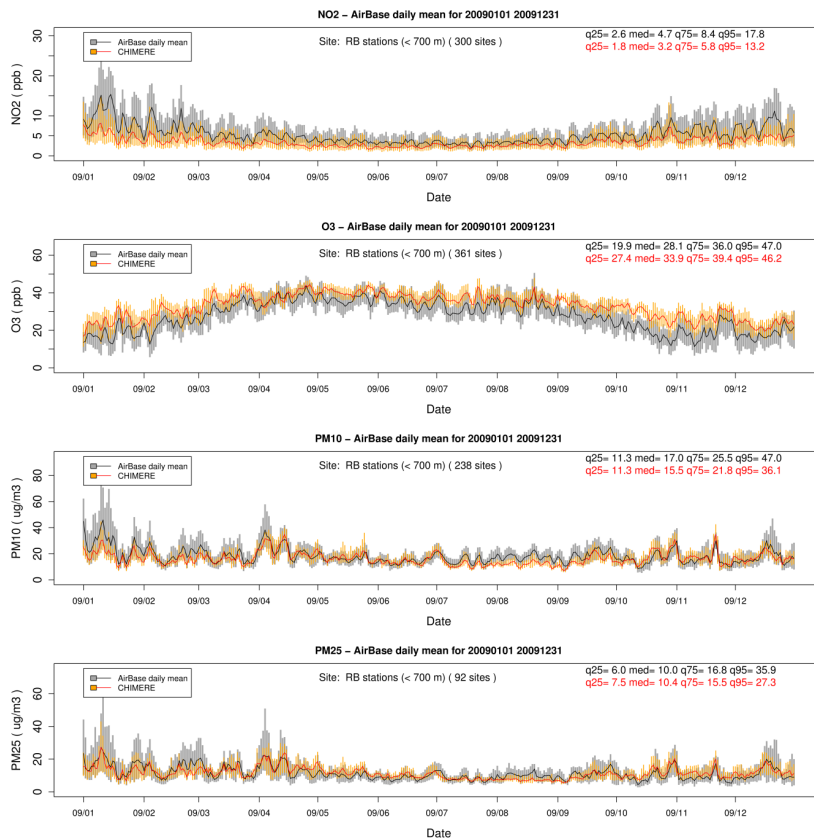


Fig. 8. Daily box-whisker plots time series of the NO₂, O₃, PM₁₀ and PM_{2.5} observed and calculated concentrations averaged over all RB Airbase stations. The continuous lines represent the medians and the bars show the 25th–75th quantile interval. The yearly 25th, 50th, 75th, and 95th quantiles are reported on the top right corner of the plots

High resolution air quality simulation over Europe

E. Terrenoire et al.

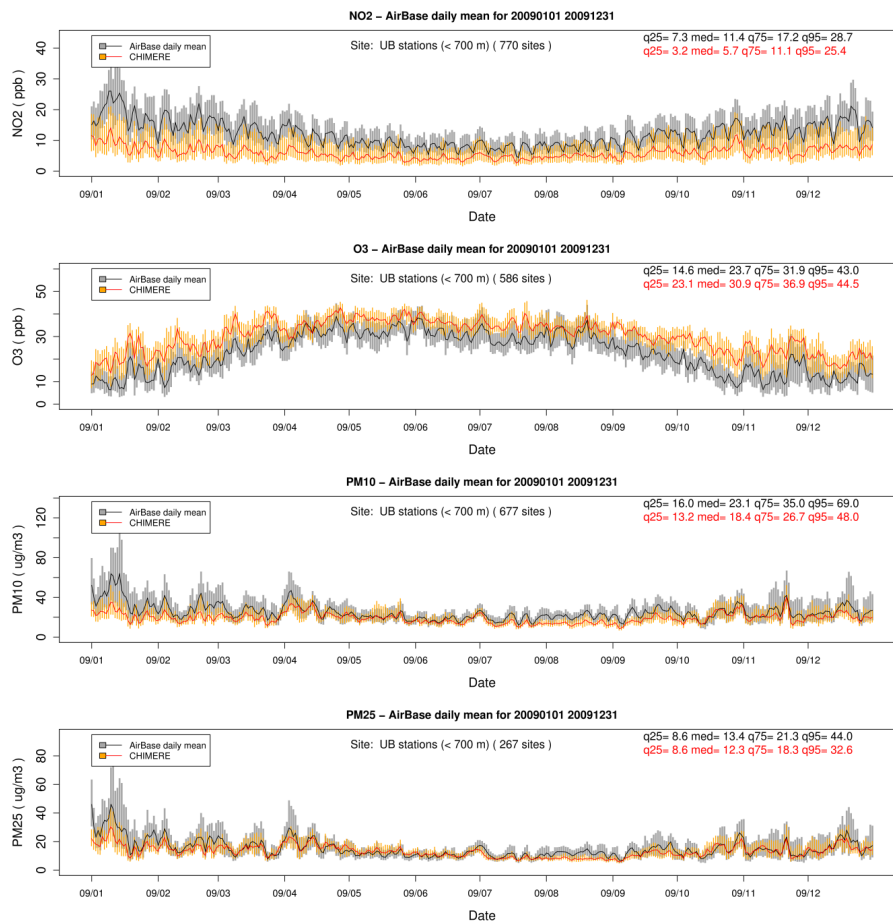


Fig. 9. Same as Fig. 8 but averaged over all UB Airbase stations.

[Title Page](#)

[Abstract](#) | [Introduction](#)

[Conclusions](#) | [References](#)

[Tables](#) | [Figures](#)

[⏪](#) | [⏩](#)

[◀](#) | [▶](#)

[Back](#) | [Close](#)

[Full Screen / Esc](#)

[Printer-friendly Version](#)

[Interactive Discussion](#)



High resolution air quality simulation over Europe

E. Terrenoire et al.

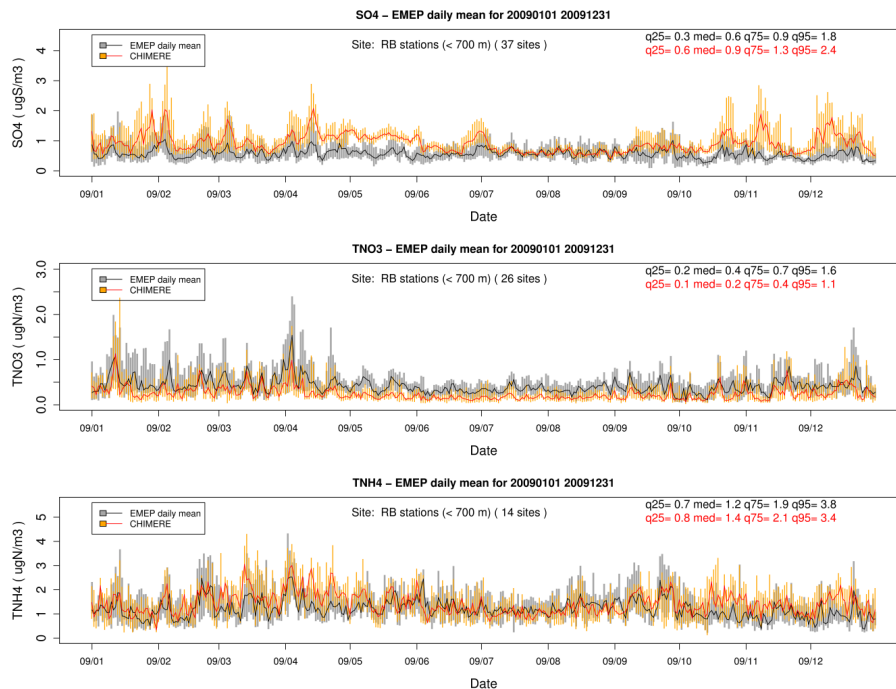


Fig. 10. Same as Fig. 8 but for sulphate, total nitrate ($\text{HNO}_3 + \text{NO}_3^-$) and total ammonia ($\text{NH}_3 + \text{NH}_4^+$) averaged over all RB EMEP stations.

Title Page

Abstract

Introduction

Conclusions

References

Tables

Figures

◀

▶

◀

▶

Back

Close

Full Screen / Esc

Printer-friendly Version

Interactive Discussion



High resolution air quality simulation over Europe

E. Terrenoire et al.

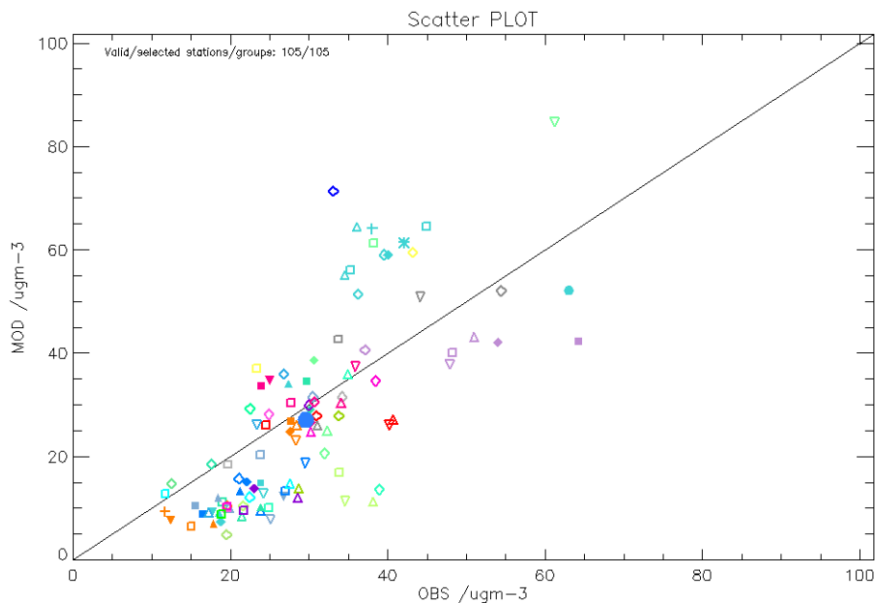


Fig. 11. Scatter plot of the modelled versus observed NO₂ concentrations ($\mu\text{g m}^{-3}$) at the UB stations ($N = 105$) of 30 major cities across Europe. The blue dot represents the mean of the 105 UB stations.

Title Page

Abstract

Introduction

Conclusions

References

Tables

Figures

◀

▶

◀

▶

Back

Close

Full Screen / Esc

Printer-friendly Version

Interactive Discussion



High resolution air quality simulation over Europe

E. Terrenoire et al.

Title Page

Abstract

Introduction

Conclusions

References

Tables

Figures

◀

▶

◀

▶

Back

Close

Full Screen / Esc

Printer-friendly Version

Interactive Discussion

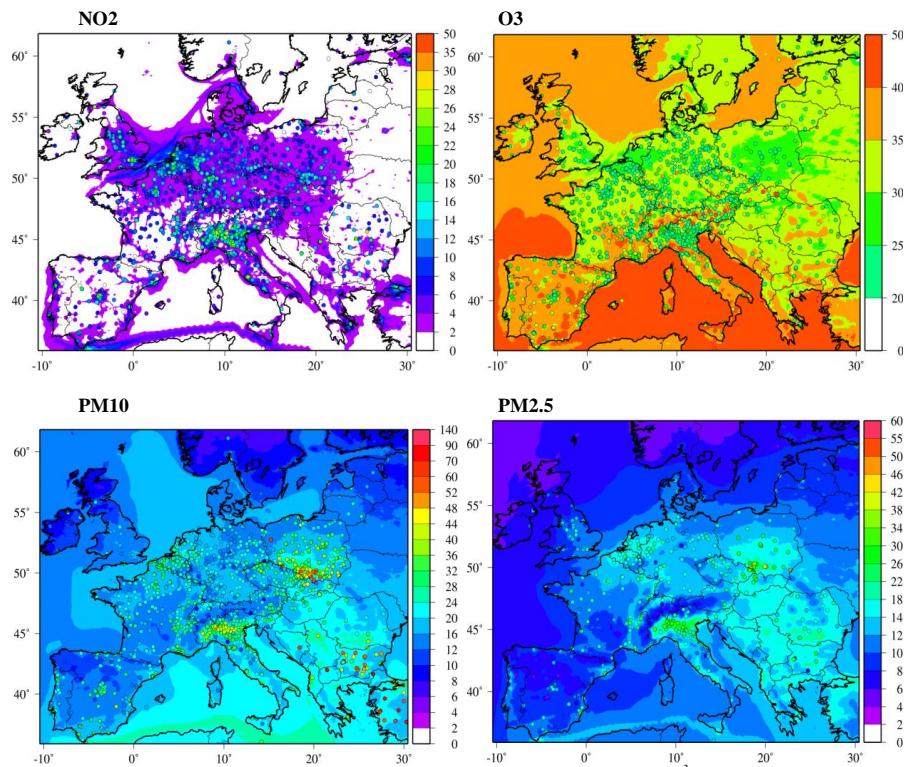


Fig. 12. Observed (dots) and modelled annual mean concentrations ($\mu\text{g m}^{-3}$) for NO₂ in ppb (top left), O₃ in ppb (top right), PM₁₀ (bottom left) and PM_{2.5} in $\mu\text{g m}^{-3}$ (bottom right).

High resolution air quality simulation over Europe

E. Terrenoire et al.

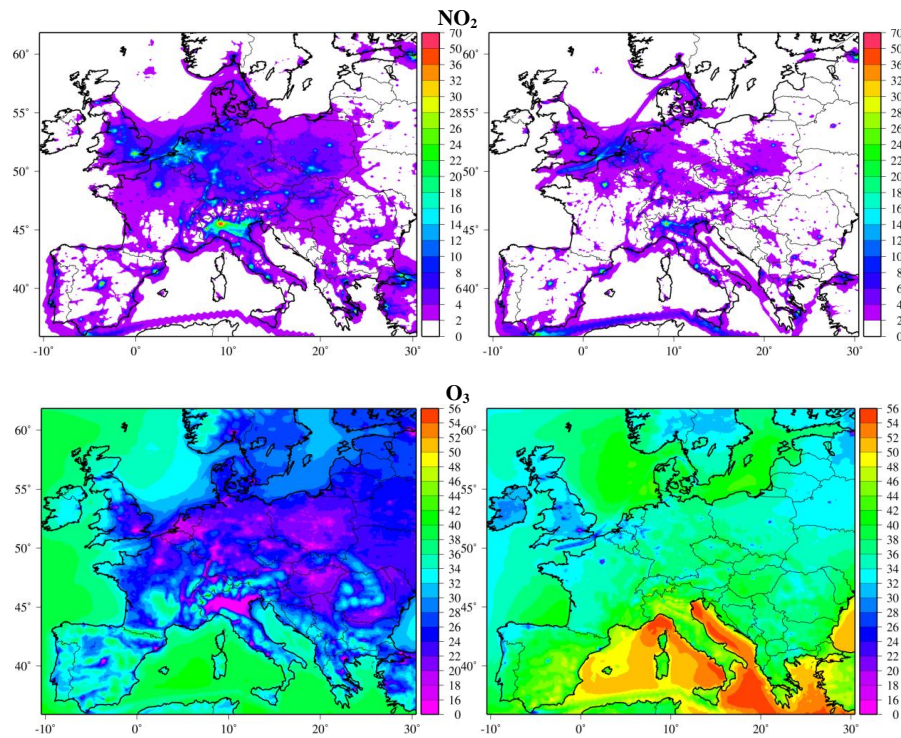


Fig. 13. Modelled NO₂ and O₃ (ppb) concentrations fields calculated for the summer (left) and the winter (right).

High resolution air quality simulation over Europe

E. Terrenoire et al.

Title Page

Abstract

Introduction

Conclusions

References

Tables

Figures

◀

▶

◀

▶

Back

Close

Full Screen / Esc

Printer-friendly Version

Interactive Discussion

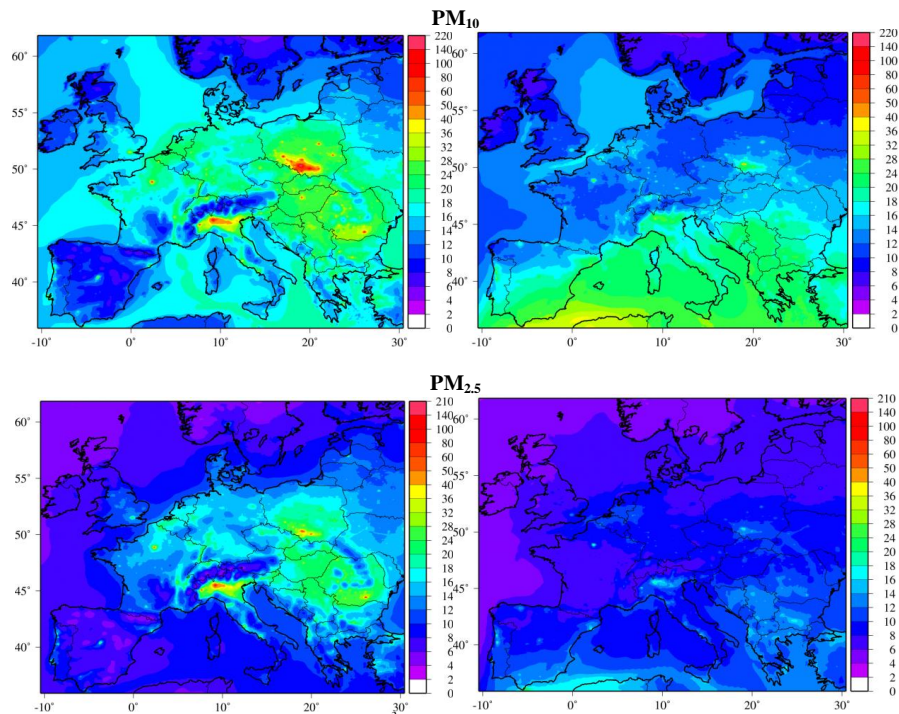


Fig. 14. Modelled PM_{10} and $\text{PM}_{2.5}$ ($\mu\text{g m}^{-3}$) concentrations fields calculated for the summer (left) and the winter (right).

High resolution air quality simulation over Europe

E. Terrenoire et al.

Title Page

Abstract

Introduction

Conclusions

References

Tables

Figures

◀

▶

◀

▶

Back

Close

Full Screen / Esc

Printer-friendly Version

Interactive Discussion

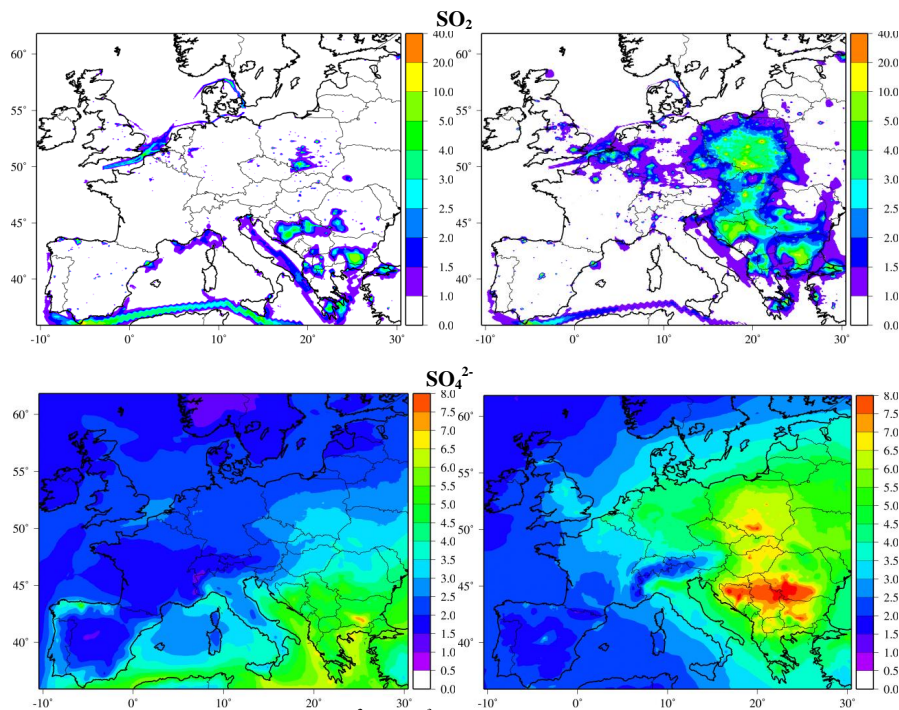


Fig. 15. Modelled SO_2 (ppb) and SO_4^{2-} ($\mu\text{g m}^{-3}$) concentrations fields calculated for the summer (left) and the winter (right).

High resolution air quality simulation over Europe

E. Terrenoire et al.

Title Page

Abstract

Introduction

Conclusions

References

Tables

Figures

◀

▶

◀

▶

Back

Close

Full Screen / Esc

Printer-friendly Version

Interactive Discussion

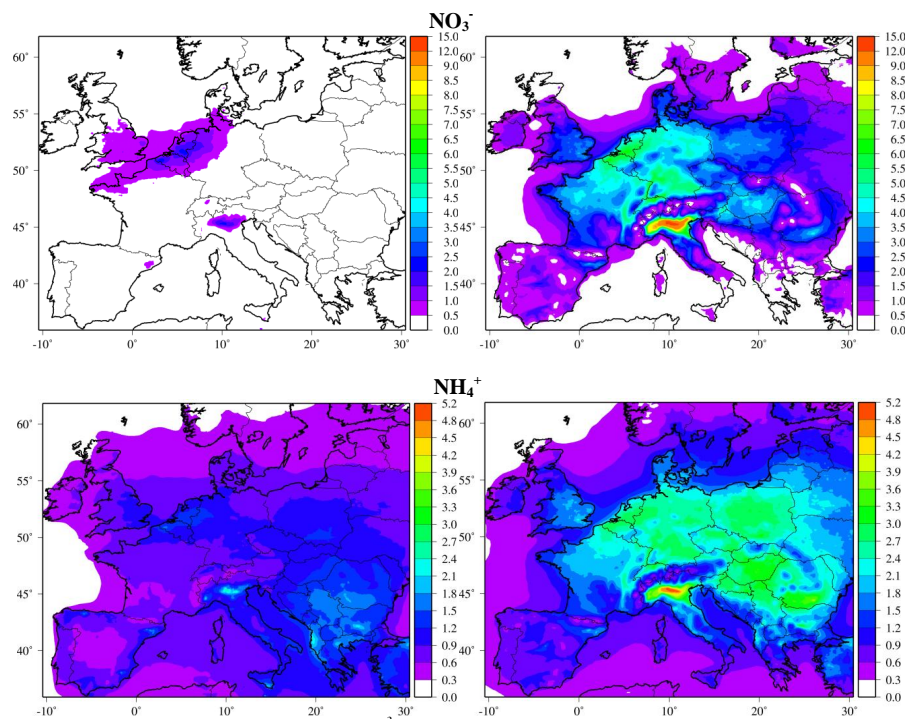


Fig. 16. Modelled NO_3^- and NH_4^+ ($\mu\text{g m}^{-3}$) concentrations fields calculated for the summer (left) and the winter (right).